Naval Research Laboratory
Stennis Space Center, MS 39529-5004

NRL/MR/7320--14-9523

Validation Test Report for NFLUX PRE: Validation of Specific Humidity, Surface Air Temperature, and Wind Speed Precision and Accuracy for assimilation into Global and Regional Models

Neil Van de Voorde
Jackie May

QinetiQ North America
Services and Solution Group
Stennis Space Center, Mississippi

Clark Rowley

Naval Research Laboratory
Ocean Dynamics and Prediction Branch, Oceanography Division
Stennis Space Center, Mississippi

December 17, 2013

Report Documentation Page

Form Approved
OMB No. 0704-0188

1. REPORT DATE	2. REPORT TYPE	3. DATES COVERED
17 DEC 2013		**00-00-2013 to 00-00-2013**

4. TITLE AND SUBTITLE	5a. CONTRACT NUMBER
Validation Test Report for NFLUX PRE: Validation of Specific Humidity, Surface Air Temperature, and Wind Speed Precision and Accuracy for assimilation into Global and Regional Models	5b. GRANT NUMBER
	5c. PROGRAM ELEMENT NUMBER
6. AUTHOR(S)	5d. PROJECT NUMBER
	5e. TASK NUMBER
	5f. WORK UNIT NUMBER
7. PERFORMING ORGANIZATION NAME(S) AND ADDRESS(ES) **Naval Research Laboratory,Oceanography Division,1101 Balch Blvd,Stennis Space Center,MS,39529**	8. PERFORMING ORGANIZATION REPORT NUMBER
9. SPONSORING/MONITORING AGENCY NAME(S) AND ADDRESS(ES)	10. SPONSOR/MONITOR'S ACRONYM(S)
	11. SPONSOR/MONITOR'S REPORT NUMBER(S)

12. DISTRIBUTION/AVAILABILITY STATEMENT
Approved for public release; distribution unlimited

13. SUPPLEMENTARY NOTES

14. ABSTRACT

15. SUBJECT TERMS

16. SECURITY CLASSIFICATION OF:			17. LIMITATION OF ABSTRACT	18. NUMBER OF PAGES	19a. NAME OF RESPONSIBLE PERSON
a. REPORT	b. ABSTRACT	c. THIS PAGE			
unclassified	**unclassified**	**unclassified**	**Same as Report (SAR)**	**55**	

Table of Contents

List of Figures

List of Tables

List of Equations

1.0 Scope

The Naval Research Laboratory (NRL) Ocean Surface Flux System Version 1 (NFLUX) provides observation processing, quality control, and analysis of measurements of ocean surface state variables for application with ocean models. The NFLUX system consists of three components: processing satellite retrievals of ocean surface state variables (NFLUX PRE), automated quality control of the observations (NFLUX QC), and 2D variational analyses of the satellite and *in situ* data with atmospheric models (NFLUX VAR). This document will review and present the current capability of the first component of the NFLUX system – NFLUX PRE. The NFLUX QC and NFLUX VAR components leverage the Navy Coupled Ocean Data Assimilation (NCODA) system to support the quality control and analysis; these two components are described in a separate report.

The NFLUX system was developed to address the requirement for accurate representation of the ocean/atmosphere interface in Navy ocean models. Unlike atmospheric models that are required to represent the entire vertical aspect of the 4D atmosphere, the NFLUX system provides products only for ocean surface state variables. The NFLUX Version 1 products are: specific humidity (Qa) at a height of 5 meters, surface air temperature (Ta) at a height of 5 meters, and scalar surface wind speed (U10) at a height of 10 meters.

Observational data sources for the NFLUX system are *in situ* ship and buoy measurements, and passive microwave Level 1b Sensor Data Records (SDRs) from: DoD the Defense Meteorological Satellite Program (DMSP) Special Sensor Microwave Imager Sounder (SSMIS), the NOAA Polar Orbiting Environmental Satellite (POES) Advanced Microwave Sounding Unit (AMSU), and European Organization for the Exploitation of Meteorological Satellites (EUMETSAT) MetOp AMSU, along with Environmental Data Records (EDRs) from the NRL Windsat instrument on the DoD Coriolis platform.

The system uses unique multiple linear regression (MLR) algorithms that have been tuned for each satellite/sensor combination using approximately two years of satellite and *in situ* observation match ups. *In situ* observations are adjusted to standard heights of 5 meters for Ta and Qa and 10 meters for wind speed using the Coupled Ocean-Atmosphere Response Experiment (COARE) 3.0 algorithm (Fairall et al., 2003).

This report documents the performance of the NFLUX PRE portion of the NFLUX system, processing raw satellite data to ocean surface measurements. The scope of the report is to examine the ocean surface products of Ta, Qa, and U10 from the passive microwave sensors on DMSP, POES, and EUMETSAT satellite systems. Data from the WindSat EDRs is presented for completeness only. Documentation of the system performance using data from the passive microwave Advanced Technology Microwave Sounder (ATMS) on the National Polar-orbiting Partnership (NPP) satellite will be

submitted as an addendum to this report when there is sufficient data for full algorithm development.

Figure 1- 1 shows the typical data coverage for Qa. The Qa product is the most extensive of the NFLUX system and uses the DMSP, POES, and MetOp satellite systems. Figure 1- 2 shows example coverage for Ta. Ta uses the POES and MetOp satellite systems. Wind speed from the DMSP satellites would be similar to the Qa coverage.

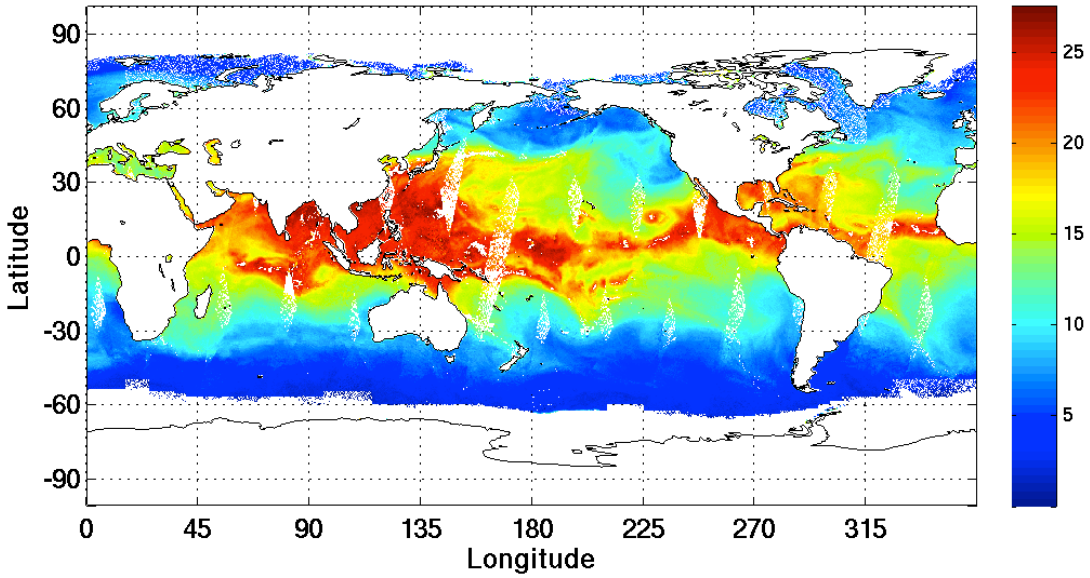

Figure 1- 1: Combined SSMIS and AMSU coverage for a single day. The data was gridded using a 0.25° mesh. AMSU satellites include N15, N18, N19, and MetOp 2; SSMIS satellites include F16, F17 and F18.

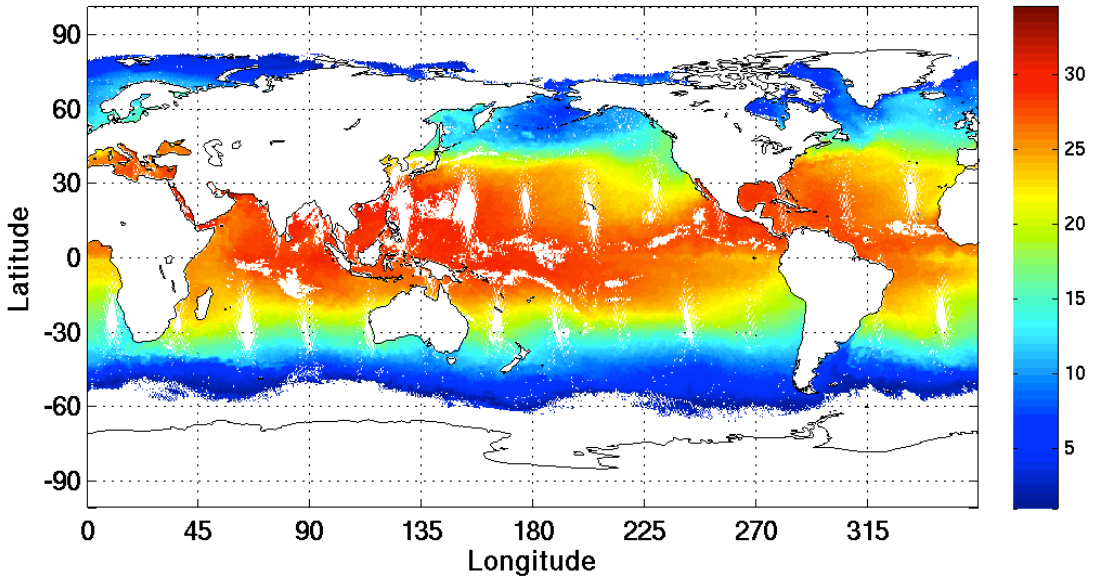

Figure 1- 2: AMSU Ta coverage for a single day. The data was gridded using a 0.5° mesh. AMSU satellites include N15, N18, N19, and MetOp 2.

1.1 Background

The initial goal of the NFLUX development was to leverage the net surface flux EDRs that were anticipated to be provided as part of the National Polar-orbiting Operational Environmental Satellite System (NPOESS). The Integrated Operational Requirements Document-II dated 14 January 2002 includes a requirement for net heat flux with a threshold for global refresh of 6 hours, an objective of 3 hours, and a latency threshold of 12 hours with an objective of 6 hours. The requirements were developed to support operational ocean modeling. Existing ocean models use the surface the net heat flux or components of the heat flux (turbulent fluxes, radiative fluxes) directly from atmospheric models or analyses, or estimate components of heat flux from combined ocean/atmosphere state variables (e.g., turbulent heat fluxes from wind speed, humidity, and air and sea surface temperatures).

NPOESS as an integrated system was cancelled. NASA and NOAA are leveraging the satellite produced by the NPOESS program – NPP. The DoD (with two remaining DMSP satellites available for launch) is examining operational requirements and risk reduction, as well as exploring smaller satellites to fulfill mission needs as a new system is developed.

Other scientific teams at various governmental and academic laboratories have put substantial effort into similar work, but mostly directed toward climate studies and climate monitoring, which do not directly support real-time operational requirements. We believe this makes the NFLUX project almost unique in its focus on supporting real-time data processing, analysis, and application in an operational forecast center environment.

1.2 System Overview

The data processing of global Qa, Ta, and U10 in the NFLUX PRE system is depicted in Figure 1- 3. The NFLUX PRE system reads the Level 1b brightness temperatures (Tb) from satellite data files and generates surface products, then combines those products with limited preprocessing of existing satellite products (i.e. WindSat) and *in situ* observations. The full suite of observations are then passed to the NCODA-based QC and VAR assimilation components.

NFLUX has four unique data sources: POES/AMSU, MetOp/AMSU, DMSP/SSMIS, WindSat, and *in situ* (ship). Each data source requires a unique reader. SSMIS and AMSU use Level 1B data, which consists of annotated engineering data that has been calibrated radiometrically to provide a geolocated Tb with a unique field of view (FOV)

for each channel along the scan path of the instrument. The ATMS is shown in Figure 1-3, but will be discussed in a future appendix to this report.

The configuration of the AMSU cross-track scanner requires unique satellite-specific corrections for each scan position and each channel. Corrections, via lookup tables, are necessary to adjust the Tb of each FOV to be equivalent to a nadir FOV (Goldberg et al., 2001). The source for the look up tables is the NOAA Center for Satellite Applications and Research (STAR). After each FOV has been extracted and corrected, the data are then 'stacked' into a two-dimensional output file. The AMSU channel Tbs are verified to be within normal limits, using values determined from a two year data set of Tbs for the channels. If any channel exceeds the min/max boundary, the Qa and Ta values are 'blanked' by replacing them with a missing value flag.

The SSMIS is a different type of passive microwave sensor that conically scans the Earth's surface and does not require the corrections that the AMSU requires. The verification of the SSMIS Tbs ranges is accomplished using a blended monthly mean for each of the imager channels with a range of three standard deviations. The static files associated with this are an external dependency. The readers include quality checks for rain, which will be discussed later in this document.

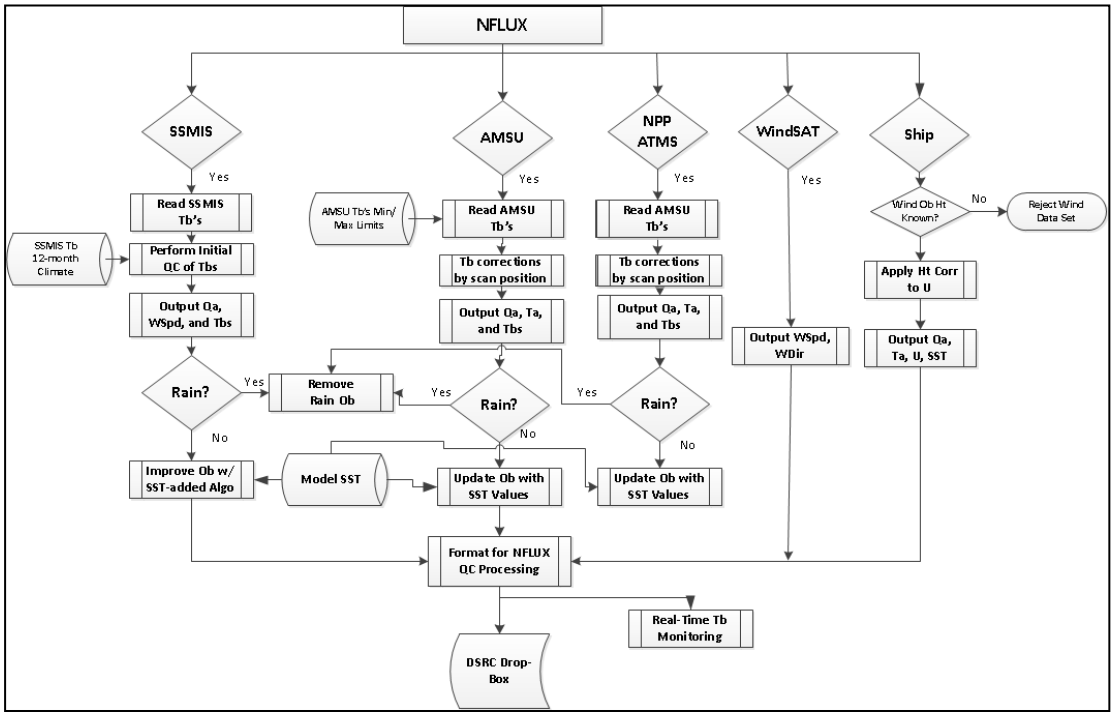

Figure 1- 3: NFLUX PRE System. The NFLUX PRE system uses Level 1B SDRs from SSMIS, AMSU, and ATMS satellite sensors. It also ingests *in situ* observations from ships and buoys as well as EDRs from WindSat. The process showing "Improve Ob w/ SST-added Algo" is the location where any region-specific algorithms are used for the NFLUX products.

The readers output flat big-endian binary files of initial estimates of Qa (SSMIS, AMSU, and ATMS), Ta (AMSU and ATMS), and U10 (SSMIS). There is a strong relationship between the sea surface temperature (SST) and of Qa and Ta and to a lesser extent U10. The initial product estimates are improved with the addition of daily model-based SSTs that are interpolated to the satellite observation position.

The ship-processing portion of the system allows *in situ* observations from ships and moored buoys to be included, based upon the availability of instrument height information associated with the platform call sign or station identification. There is an external dependency for a database file with height of observations; the observation heights in this database are from the National Data Buoy Center (NDBC) web site and the World Meteorological Organization (WMO) Publication No. 47 (Kent et al., 2007). When there is complete set of observations from a station, specific humidity is calculated using the air temperature and dew point observations. The ship/buoy reader includes the COARE 3.0 algorithms (Fairall et al., 2003) to adjust the surface parameters of wind speed, air temperature, and specific humidity to heights of ten (10), five (5), and five (5) meters respectively. If there is insufficient information to use the COARE algorithm (e.g., only a wind speed observation), no height adjustments are made.

The last component of the NFLUX PRE system is the WindSat EDR reader. The wind speed and direction are output from the reader and are available for processing through the NFLUX QC program.

2.0 System Components

2.1 Data Feeds and Data Description

There are three types of data feeds for the NFLUX PRE system: SDR, EDR, and ship or buoy surface observations. SDRs include the DMSP SSMIS sensor, the POES and MetOp AMSU sensor, and the NPP ATMS sensor. EDRs are from the WindSat on Coriolis. Ship and buoy observations are from a near-real time NAVOCEANO database pull and are equivalent to an EDR. Table 1 shows a brief summary of the platform, sensors, and products within the NFLUX system. The Local Time of Ascending Node (LTAN) crossing is included as an indication of the temporal coverage of the satellite systems.

Table 1: NFLUX platforms and products. The NFLUX system uses three types of data feeds: SDRs from four different satellite systems (i.e. DMSP, POES, MetOp, and NPP), EDRs from WindSat, and *in situ* observations from ships and buoys.

Platform/ID	Spec Humidity	Wind Speed	Air Temp	Local Time Ascending Node (LTAN)	Notes
DMSP/SSMIS					
F16	X	X		21:32	
F17	X	X		17:36	
F18	X	X		20:00	
POES/AMSU					
N15	X		X	16:41	
N18	X		X	14:00	
N19	X		X	13:34	
MetOp A	X		X	9:30	
MetOp B				9:30	
NPP/ATMS					
NPP	X		X	13:30	
CORIOLIS					
WindSat		X		18:00	
Surface Obs					
Ships	X	X	X	n/a	
Buoys	X	X	X	n/a	

The readers fall into two general categories: one for binary data files, and one for HDF5 files. Currently, the only HDF5 reader is for the ATMS on NPP. The data files for all other inputs are read as flat binary files in either big or little endian. SDR readers can output products using two sets of sensor channels. If the full complement of channels is available, they are used. If only the imager channels are available, then they are used. Table 2 shows the channels that are available for product development.

Table 2: SDR Channels for SSMIS and AMSU passive microwave sensors. The 91 and 183 GHz channels for SSMIS are only available for odd numbered scans within the SDR.

Channel	Imager/ Sounder	Imager- Only	SSMIS	AMSU
1	X	X	19.35 GHz (V)	23.8 GHz
2	X	X	19.35 GHz (H)	31.4 GHz
3	X	X	22.235 GHz (V)	50.3 GHz
4	X	X	37.0 GHz (V)	52.8 GHz
5	X	X	37.0 GHz (H)	53.596 GHz
6	X		91.655 GHz (V)	89.0 GHz
7	X		91.655 GHz (H)	---
8	X		183.3 ± 3 GHz	---

2.1.1 SSMIS

The SSMIS data reader processes data for Tbs at 19 GHz (vertically and horizontally polarized, V/H), 22 GHz (V), 37 GHZ (V/H), 91 GHz (V/H), and 183.3 +/- 3 GHz (H) for a total of eight brightness temperature channels. The reader also uses the SDR surface types embedded in the data record for each FOV and only allows 'near coast' or 'ocean' views to pass through. The SSMIS SDR format document was downloaded from http://www.ncdc.noaa.gov/oa/rsad/ssmi/ssmi.html, AE-26775E, dated 07NOV2005.

Unique to the NFLUX SSMIS reader, is an FOV remapper for the 91.6 and 183.3 GHz sounder channels that produces a geographically weighted match at the nominal size of the imager FOVs. This was constructed using a 5 x 4 FOV weighting scheme based on a simple trapezoid rule. These higher frequency channels are only available on odd numbered scans within the SDR. If scan lines are missing, the interpolation/weighting fails and a remapped brightness temperature is not produced. In this case the algorithm that relies solely on the imager channels is selected for use.

Initial quality control is accomplished using external files of monthly mean climates and their variability for the first five brightness temperatures, as listed in Table 2. The mean error (ME) and three standard deviations (SD) are interpolated to the observation day from adjacent monthly values. If all of the lower five channels fall within the boundaries of the ME ± 3SD, then the observation is passed through. Otherwise it is set to a missing value flag of -999.

Additional quality control is accomplished through the use of two separate rain flag indictors. The 37 GHz rain flag, equation (1), is based upon Goodberlet et al. (1990 and 1992). It uses the difference between the vertically and horizontally polarized 37 GHz brightness temperatures.

$$RF37 = Tb_{V37} - Tb_{H37} \tag{1}$$

The scattering index (SI) rain flag is based on Grody (1991). It was developed for the SSM/I sensor using the 85 GHz channel. The SSMIS uses a 91 GHz channel in place of the 85 GHz. Equation (2) shows the formula used.

$$SI_{SSMIS} = 450.2 - 0.506(Tb_{V19}) - 1.874(Tb_{V22}) + 0.00637(Tb_{V19})^2 - Tb_{V91} \tag{2}$$

The observations that are flagged as rain-contaminated are removed within the software component that adds the background SST model values into the product calculation. If the difference between the 37GHz channels exceeds 37 (i.e. low probability of rain contamination) and the value of SI is less than 10, the observation is assumed not to be rain-contaminated. The observation is then output to the NFLUX QC processing system discussed in a separate document.

2.1.2 AMSU

The AMSU brightness temperature channels used in the NFLUX system are: 23.8 GHz, 31.4 GHz, 50.3 GHz, 52.8 GHz, 53.6 ± 0.1 GHz, and 89.0 GHz, as shown in Table 2. The polarization of the channels is quasi-vertical, with the exception of the 53.6 channel, which is quasi-horizontal (NOAA KLM User's Guide, Section 3.3) .

The AMSU SDR reader is based on a program provided by W.D. Braswell at the National Space and Technology Center, University of Alabama Huntsville (personal communication, 2006). The baseline program was expanded to perform the limb corrections, corrections proposed by Mo (1999), and to add land/sea masking. The AMSU reader has additional code to read the ARS header discussed in the NOAA User Manual (http://www.ncdc.noaa.gov/oa/pod-guide/ncdc/docs/klm/html/c8/sec831-2.htm, accessed 17 August 2012).

Quality control within the reader is accomplished using channel-specific minimum Tbs and a common maximum Tb for each channel. If all of the channels fall within the min/max boundaries, then the observation is passed through. These values were established using a large set of matched *in situ* observations and channel brightness temperatures.

The two rain flags used for the AMSU sensor are based on Hu et al. (2006). The first rain flag uses a simple threshold in the Tb_{89} channel. If Tb_{89} is greater than 254.56K, it is

assumed to be rain contaminated. The scattering index rain flag is shown in equation (3). If the SI is greater than 9, the pixel is assumed to contain rain.

$$SI_{AMSU} = -113.2 + (2.41 - 0.0049Tb_{23})Tb_{23} + 0.454Tb_{31} - Tb_{89} \quad (3)$$

Similar to the SSMIS data, the rain-flagged data is carried through the reader but is filtered out within the software routine that adds the background SST model values into the product calculation.

2.1.3 ATMS

The ATMS sensor is onboard the NPP satellite. The reader for the data processes all 22 brightness temperature channels. ATMS duplicates and expands the available channels on AMSU along with its companion sensor the Microwave Humidity Sounder (MHS). The 89.0 GHz AMSU channel has been replaced with an 88.2 GHz channel and a 51.78 GHz channel is also available.

The ATMS retrieval characteristics, validation, and verification will be submitted as an appendix to this report at a later date.

2.1.4 WindSat

The WindSat is a polarimetric microwave radiometer instrument on the Coriolis satellite. It is a unique satellite/sensor and was intended to be a three- to five-year demonstration project for the DoD. Distinct to this satellite/sensor, EDRs are utilized rather than the SDRs. The EDR is comprised of data records spaced in time for every fourth 37 GHz (V/H) measurement. The EDR is available in three different resolutions. The selection of the lower resolution product is discussed in section 3.3.5. The reader uses the EDR values of the QC flags for rain, ice, land, and lake to filter out rain- and ice-contaminated observations, and observations over land or lakes. The EDR contains four possible solutions to the direction ambiguity associated with the data processing. The single solution with the highest ranked value available in the EDR is selected.

The WindSat data is incorporated into the NFLUX system, but its inclusion in this description of the NFLUX PRE component is for completeness only. The reader for the WindSat EDR was downloaded from: http://www.emc.ncep.noaa.gov/mmb/data_processing/satellite_ingest.doc/File_Format.doc/WindSat%20Environmental%20Data%20Record%20files%20from%20NAVOCEANO.htm.

2.1.5 Ship and Buoy

The NFLUX system also utilizes *in situ* observations processed at the Naval Oceanographic Office or another operational center, most of which are obtained from the World Meteorological Organization (WMO) Global Telecommunication System **(**GTS**)**. Observations of wind speed, wind direction, Ta, Qa, and SST are output. The Qa value is determined using the reported dew point temperature and surface pressure reading:

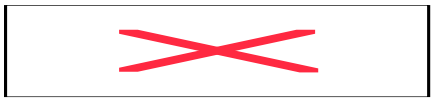

(4)

where vp is the surface vapor pressure, $P_{surface}$ is the surface pressure in millibars, and T_{dewpt} is the dewpoint temperature in ^{o}C. The ship reader was developed to read the *in situ* data files from NAVOCEANO-formatted files. Only NAVO-assigned types of 71 (i.e., ship) or 73 (i.e., buoy) are processed. The format used is based on the Real-Time Data Handling System (RTDHS) format dated 06-30-04. The reader is presently hard-coded to skip over any observation with classification other than UNCLASS. There are presently five black-listed buoys (call signs 52082, 52085, 52088, 31007, and 13001), based upon their anomalous observation records. These are hard-coded exclusions contained in the reader program.

Ship and buoy observations are recorded at various heights. Ship observation heights are provided by the World Meteorological Organization (WMO) Publication No. 47 (Kent et al., 2007). Buoy observation heights are from the National Data Buoy Center (NDBC) web site. Observations from buoys that do not have a listed observation height are processed and assumed to have an observation height such that any adjustments to the standard 5/10 meter heights would be minimal. If a ship call sign is not in the database extracted from the WMO Publication 47, the values for heights by vessel type listed in Kent et al. (2007) are used. If no vessel type is available, then the platform is assumed to be a standard container ship, and the processing uses nominal values from Kent et al. (2007) for heights of observation (specifically, an anemometer height of 37.4 meters, an air temperature sensor height of 28.8 meters, and an SST depth of 7.2 meters).

Incorporated in the *in situ* data reader is a module containing the COARE 3.0 algorithm (Fairall et al., 2003) to adjust all *in situ* observations to standard 5/10 meter heights. The COARE subroutine uses an assumed downward solar flux of 1000.0 wm^{-2} and a downward infrared flux of 400 wm^{-2}. The observations of Ta, Qa, and wind speed are adjusted, when possible, to standard heights of 5 meters for Ta and Qa and 10 meters for wind speed. The COARE algorithm assigns invalid values of -99.3 to Ta, Qa, and wind speed when it cannot calculate a height-adjusted measurement.

2.2 Utility Programs

Included in the NFLUX system is a utility program that can provide a real-time monitoring of the satellites channels, TB_trace. The TB_trace program operates on the output from the SSMIS and AMSU readers. The program extracts out the brightness temperatures associated with a narrow band of specific humidity values (i.e., 14.9 and 15.1 g kg^{-1}) for each satellite and appends that information to an existing ASCII output file. The output format is: DTG, the satellite ID, the number of observations for that satellite, and then either six channels for AMSU or eight channels for SSMIS with the mean and standard deviation of the data.

Figure 2-1 shows an example of the TB_trace output using the AMSU data. The mean (blue) and standard deviation (red) of the brightness temperatures for each of the six imager channels are shown. The purpose of this program is to allow a rapid and simple visualization of the performance of the various imager channels. A degrading or drifting channel is presumed to be apparent in the 'trace' of the data.

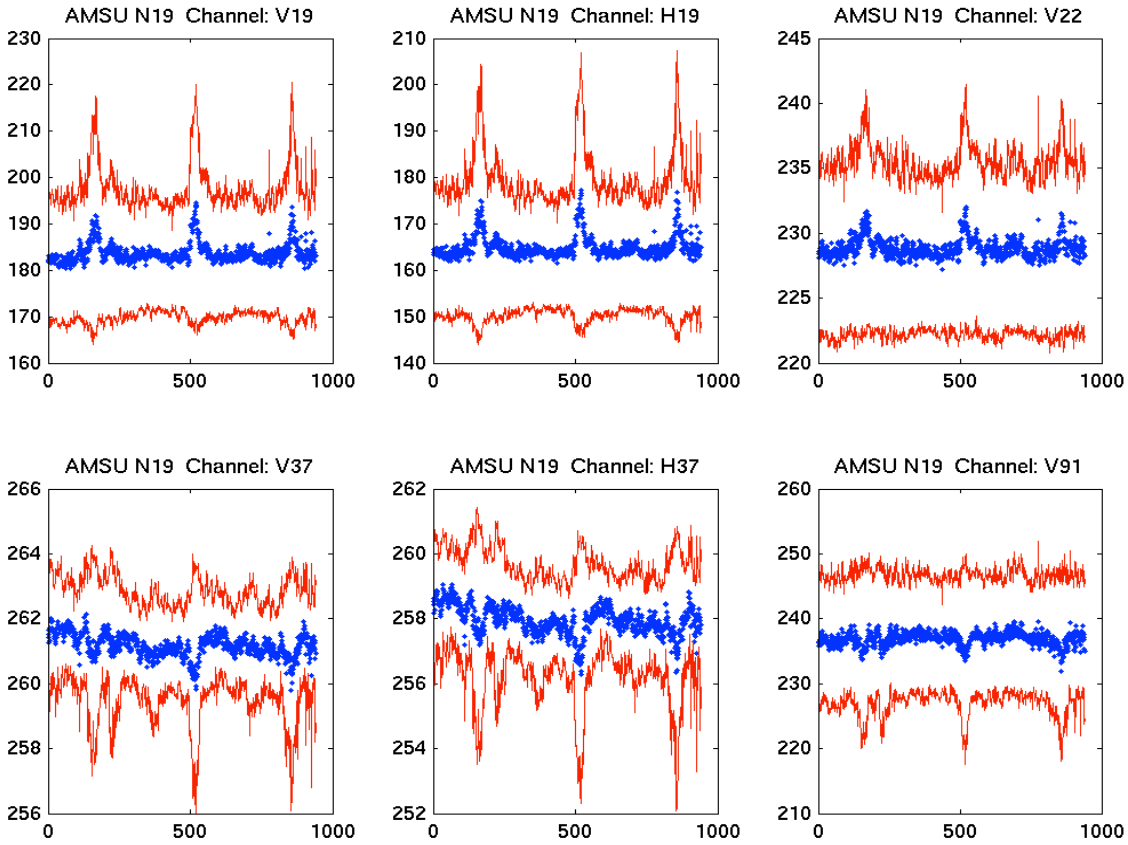

Figure 2-1: Output from TB_Trace.f90 program showing the range of brightness temperatures for the 6 AMSU channels associated with a calculated specific humidity of 14.9 to 15.1 g kg^{-1}.

3.0 Algorithms

3.1 Development

All of the algorithms use a multiple linear regression (MLR) technique using the available satellite brightness temperature channels, shown in Table 2. The table shows which channels are used for the combined imager/sounder algorithm and which channels are used for the imager-only algorithm. The primary distinction between the two types for the SSMIS algorithms is the need for the sounder data, which is only produced for odd scan lines within the data. There are two stages used in the construction of an NFLUX product: an initial satellite-only product estimate, and a subsequent estimate using a background SST value. The SST values are presently obtained from the NAVOCEANO 10 km (K10) global SST composite used in the operational SST retrieval processing.

Each algorithm was developed independently for each satellite/sensor. *In situ* observations from ship or buoy data from Jan 2010 through Dec 2011 (24 months) were matched to corresponding satellite passes. Satellite observations were initially required to be within one degree of longitude and latitude and within six hours of the *in situ* data. These were then filtered down to a one-to-one match up based on the satellite observation that was closest in time and space to the *in situ* data.

The two-year sets of ship/buoy observations, along with the selected satellite Tb channels, were binned every five units (e.g., 0-5, 5-10, … g kg^{-1} for specific humidity), from 0 through 30. A number of matched observations and Tbs were randomly selected to populate each of the bins. The combined bins were then equally divided into subsets to be used for training and verification. The number of observations placed into the bins was based on the number of observations in the 0-5 bin. For AMSU and SSMIS, this ranged from 6000 to over 10000. This bin typically represented the smallest sample used in the resampling of the data with the exception of the very high bins.

Early in the development of the algorithms, it was noted that each resulting training and verification data set had slightly different MLR coefficients. In order to handle the sample variability, a bootstrapping technique was employed, in which the regression process was repeated 2000 times. This provided a robust sample for each of the brightness temperature channels from which the mean of each was selected as the coefficient. The distributions for the regression coefficients tended to be unimodal. Figure 3- 1 shows the distributions for the DMSP F18 Qa coefficients.

The Qa (AMSU and SSMIS) and U10 (SSMIS) algorithms require additional processing. The Qa algorithms showed limited skill in estimating observed values above 18 g kg^{-1}. This was attributed to the response of one or more of the microwave channels ceasing to be linear with increasing moisture. The SSMIS response to changing wind speed is a complex issue that is a function of the foam and roughness of the ocean surface (Hwang,

2012). In each case, an internally consistent adjustment scheme was developed. No external information is required for these adjustments.

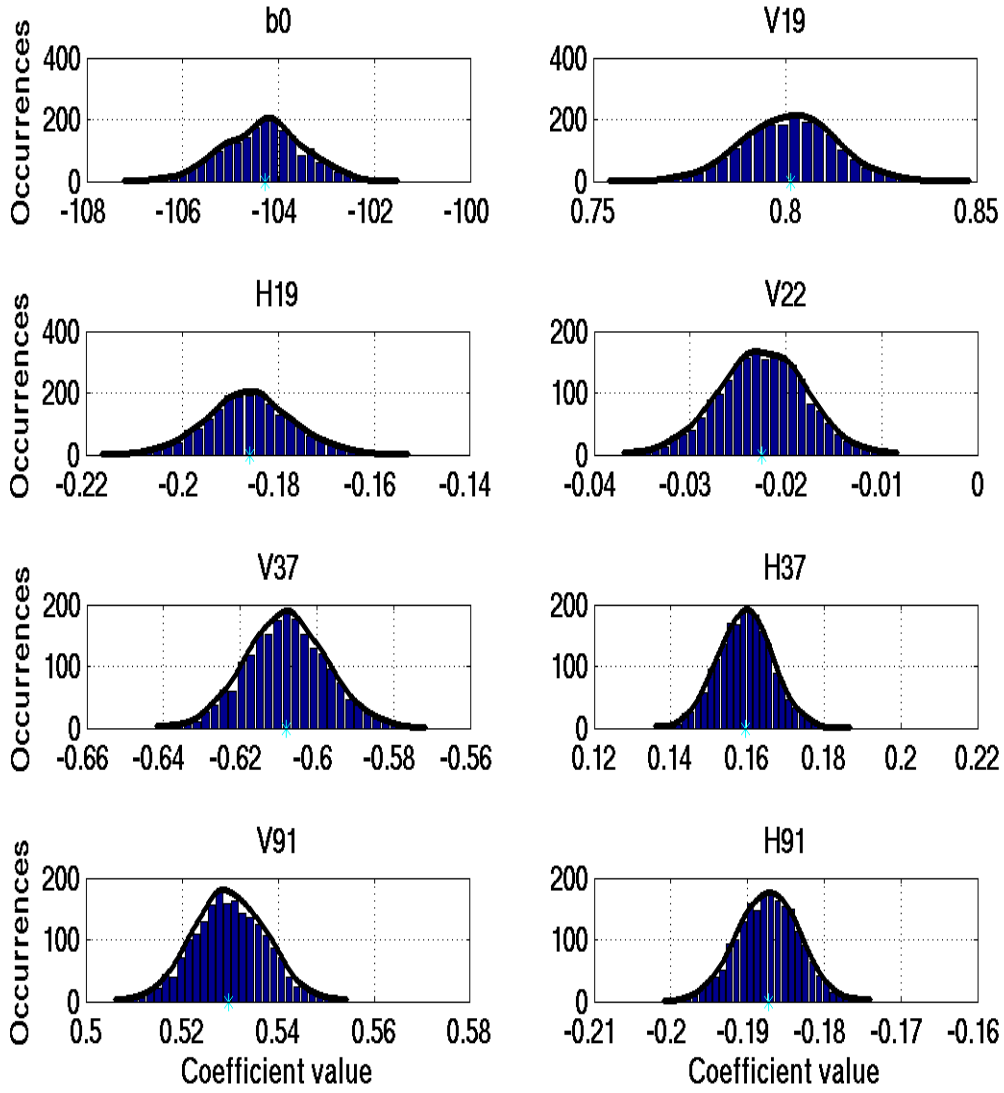

Figure 3- 1: Example of the bootstrapped MLR coefficients for the QA product from DMSP F18. 2000 sets of randomly-sampled MLR coefficients where used to selected the most-probable coefficient, as indicated by the '*" along the x-axis, for the particular satellite and channel.

For the Qa adjustment, an incremental factor was established for each of the AMSU and SSMIS products. The adjustment for AMSU is:

 (5)

where β is a satellite-specific weighting function, ranging from 0.5 to 2.0 and $Tb_{\overline{52.8}@Qa=16}$ is the average brightness temperature for the 52.8 (53.6) GHz channel calculated using a range of 15.9 to 16.1 g kg^{-1}. These values for both the vertically and horizontally polarized channels are fixed for each satellite/sensor. The SSMIS Qa adjustment is:

$$\Delta Qa = \begin{cases} 0, & if\ Tb_{V22} < 240K \\ \beta\left(Tb_{V22}^2 / 240\right)^2 \left(Tb_{V22} - 240\right), & if\ Tb_{V22} > 240K \end{cases} \quad (6)$$

where β is less than 1.0 for all of the DMSP/SSMIS satellites.

The adjustment for wind speed is a double-step application that bias corrects the output across the entire range of wind speeds. The adjustments were calculated based on differences between the *in situ* data and the initially-calculated SSMIS wind speed. The differences were binned and the mean bias of each difference bin was used to create a second-order correction that is added to each initial satellite observation.

$$\Delta Ws_1 = c_o + c_1 Ws_{init} + c_2 Ws_{init} \quad (7)$$

where the c_o, c_1, and c_2 are calculated uniquely for F16, F17, and F18. The increment ΔWs_1 is added to the initial U10 value and the process is repeated once more with another set of coefficients. This process resulted in a decrease in the initial estimated wind speed for low speed conditions and an increase in wind speed for higher conditions and an overall improved U10 product.

The inclusion of model-based SSTs in the algorithm improved the overall performance of the system. This was most prevalent in the air temperature estimate, followed by specific humidity and then to a lesser extent wind speed. The source of K10 SST was selected over the available K100 (100 km global) SST composite product in part because it provided a suitable ice mask in high-latitude regions and the NFLUX PRE product-level statistics were marginally better than the K100-based products. The system retains the latent ability to utilize the K100 SST files. The inclusion of the K10 SST information results in a recalculation of the NFLUX product for each satellite FOV.

3.2 Product Precision

The precision for each of the three products from the two sensor types (AMSU and SSMIS) was estimated using the standard deviation of matched-up satellite observations to ship/buoy observation clusters. Clusters include all satellite observations within six hours and one degree around a ship observation. The clusters were used to estimate the precision for each of the satellite products; see Table 3. The estimates were based on the unbiased standard deviation of the clusters of satellite observations around a single ship

observation. The mode of the distribution of the standard deviations was selected as the precision.

Table 3: NFLUX Product Precision. The precision of each of the NFLUX products was estimated using the match-up databases before filtering to a single nearest match up.

Sensor	Surface Product	Precision
SSMIS	Wind Speed	0.67 m s^{-1}
	Spec Humidity	0.44 g kg^{-1}
AMSU	Spec Humidity	0.30 g kg^{-1}
	Air Temperature	0.25 ^{o}C

3.3 Product Accuracy

The accuracy of the NFLUX products was measured using the standards of mean error (ME), standard deviation (SD), root mean square error (RMSE), and correlation coefficient (R^2). The basis for the comparison was the difference between the matched up satellite observation and the *in situ* observation. As discussed above, the matched up satellite observation was the closest observation in distance and time in a cluster that was within 1^{o} and within six hours. Additionally, the data was filtered to have a minimum distance to land of 111 km and an NFLUX QC value of 0.90 or less.

The accuracy of each of the products was assessed using similar tools to those that were used to construct the match-up data set for algorithm development. Table 4 shows recent estimates of the mean error from the Voluntary Observing Ships (VOS) program from 1970 to 2002 (Kent and Berry, 2005, and Kent et al. 2007). Roughly 78% of the *in situ* observations were from buoys. Gilhousen (1987) found that for NDBC buoys the wind speed bias was less than 0.1 m s^{-1} over a range of wind speeds less than 25 m s^{-1}, with a standard deviation of less than approximately 1 m s^{-1} over the same range. Air temperature errors were reported to have a very small negative bias (i.e. -0.03 ^{o}C) with a standard deviation of less than 0.1 ^{o}C. No error was estimated for specific humidity.

Table 4: Global estimates of random observational errors from Kent and Berry (2005). The table shows the difference between the observations without regard to the height of the sensors and the local atmospheric stability, and the observations adjusted to a common 10-meter height.

	Mean Error	
Variable	**Unadjusted Ob**	**Adjust Ob (neutral 10 meter ht)**
Specific Humidity (g kg^{-1})	1.1 ± 0. 1	1.0 ± 0. 1
Air Temperature (^{o}C)	1.4 ± 0. 1	1.1 ± 0. 1
Wind Speed (m s^{-1})	2.3 ± 0. 1	2.0 ± 0. 1

The height of observation varies greatly in the database, especially those from ships. This was addressed by adjusting the parameters to a standard level. The COARE 3.0 algorithm (Fairall et al., 2003) was used with a standard height of five meters for air temperature and specific humidity and 10 meters for wind speed. In the case of buoys where there were no wind speeds in the observation data set, there was no height adjustment. An analysis of the buoy heights of observations indicated that the heights of observation typically ranged from three to five meters. Based on the adjustments calculated using the COARE 3.0 algorithm, a non-adjusted three- to four- meter observation was accepted as being equivalent to an adjusted five meter observation height for the match-up database. All of the ship observation data for Qa, Ta, and U10 were processed through the NFLUX QC program, and only those with an assigned error probability less than 0.90 were used for the comparisons and in the satellite algorithm development.

3.3.1 SSMIS QA

The NFLUX SSMIS Qa product performance indicators are shown in Figure 3- 2, Figure 3- 3, Table 5, and Table 6. The global distribution of the 284462 observations (Figure 3- 2, upper left panel) indicates global coverage except for extreme southern high latitudes. The bias distribution of both the NFLUX SSMIS Qa and corresponding NOGAPS Qa to ship/buoy observations is shown in the upper right panel of Figure 3- 2. The SSMIS Qa bias is 80% lower than the NOGAPS bias (i.e. -0.21 versus -1.07 g kg^{-1}). There is an 83% probability of NOGAPS underestimating the humidity at the ocean surface, based on the histogram of the bias. The NFLUX probability is much more Gaussian in shape, with a cumulative negative bias of 62%.

Scatter plots of the NFLUX and NOGAPS match-ups to ship/buoy observations are shown in the lower figures of Figure 3- 2. The distribution of the scatter is shown by relative colors, with the warmer colors indicating a greater concentration of data. The NOGAPS (lower right panel) performance shows a strong correlation; the correlation coefficient is 0.903, throughout the lower two-thirds of the Qa range. The asymmetry of the NOGAPS bias discussed above is evident in the distribution. Also evident in the distribution is the asymptotic behavior at higher moisture levels, with a practical limit of about 19 g kg^{-1}. Less evident, but still present, is the asymptotic behavior at very low moisture levels. For the NFLUX distribution (lower left panel), the greater degree of symmetry in the scatter plot is evident, but with a lower correlation coefficient, 0.859. At higher moisture levels, the asymptotic behavior noted in the NOGAPS distribution is not present; visually, the correlation remains fairly strong (the thick black line shows the one-to-one correlation line). The increased scatter of the moisture value is due to the correction that is applied to the retrieval (when the brightness temperature of the 22 GHz channel exceeds 240K; see equation (6)). Table 5 shows the summary of the global performance of the NFLUX SSMIS Qa and the matched up NOGAPS Qa products. The performances of the individual SSMIS sensors are also indicated.

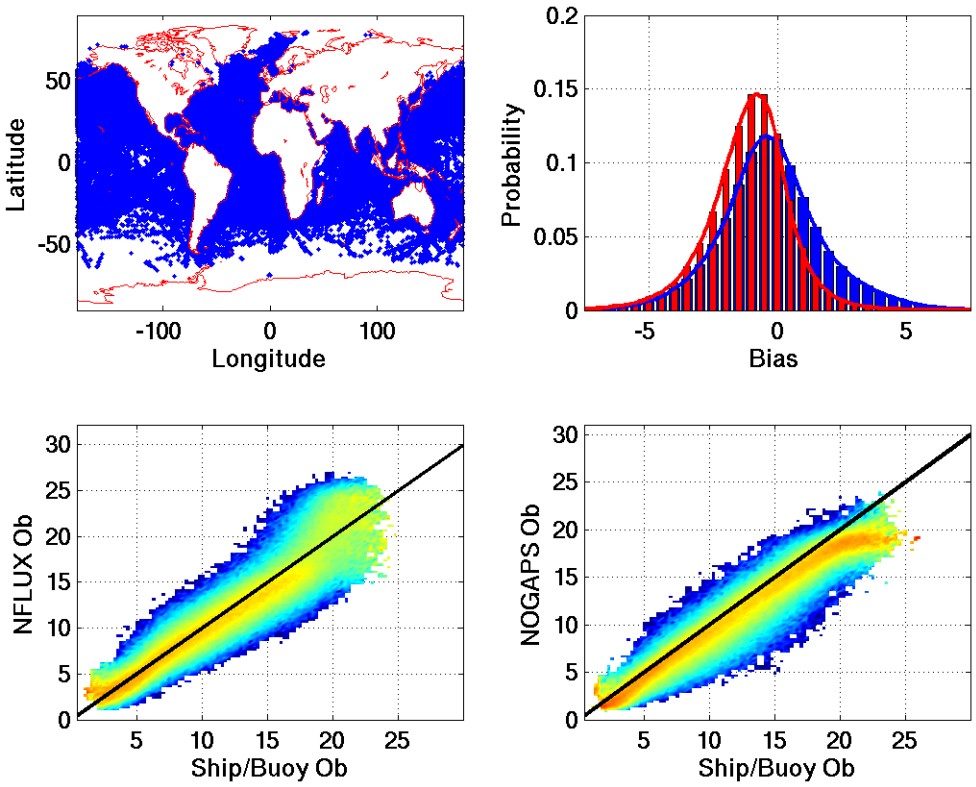

Figure 3- 2: 4-Panel SSMIS Qa Performance Summary. The upper left panel shows the distribution of the matched up observations. The upper right panel shows the distributions of NFLUX minus ship/buoy observations (blue) and of NOGAPS minus ship/buoy distribution (red). The lower left panel shows the NFLUX scatter plot that has been shaded to show the relative distribution of the scatter. The increased scatter above the ship/buoy observation of 15 g kg^{-1} is associated with the high Qa correction based on the 22 GHz (V) channel. The thick black line shows a one-to-one correlation for visual reference. For comparison the NOGAPS scatter plot is shown in the lower right panel.

Table 5: SSMIS Qa Product Performance. A total of 284462 match ups were generated from January 2010 through July 2012. The mean error/bias (ME), standard deviations (SD), and root mean square error (RMSE) estimates for the NFLUX product are compared to the NOGAPS values associated with the observation location and time of the satellite data. The individual satellite performance values are also indicated.

SSMIS Qa				
	ME	**SD**	**RMSE**	**R^2**
NFLUX	-0.2183	2.0373	2.0489	0.8594
NOGAPS	-1.0744	1.6174	1.9417	0.9030
Satellites				
F16:	-0.2218	2.0964	2.1081	0.8568
F17:	-0.1566	2.0709	2.0768	0.8583
F18:	-0.2503	1.9843	2.0000	0.8615

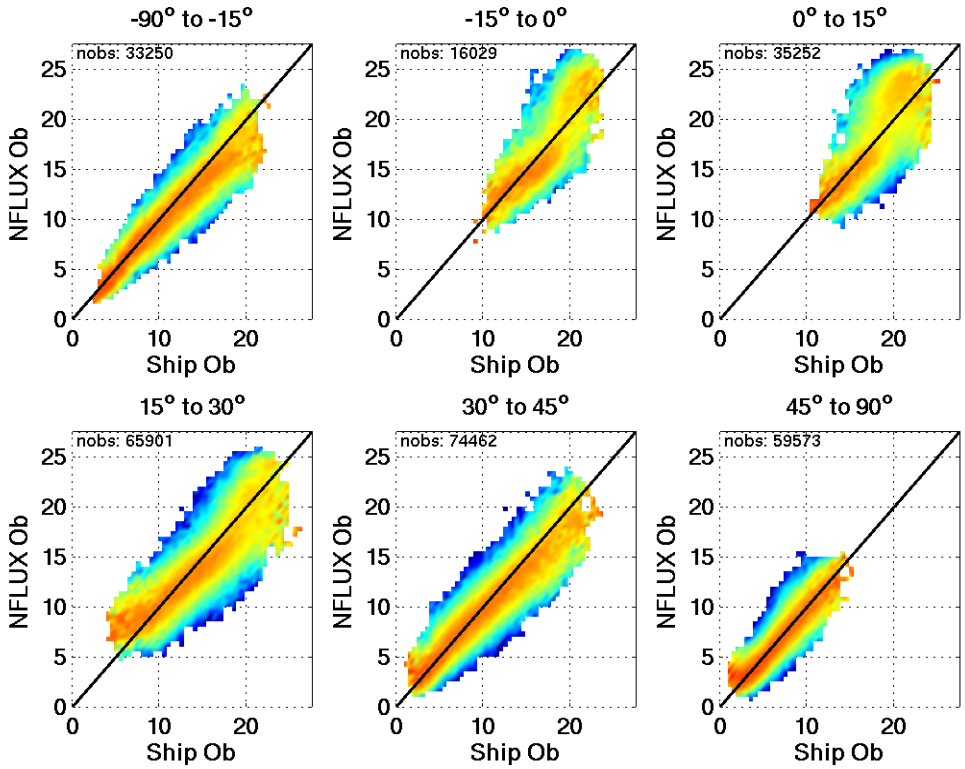

Figure 3- 3: 6-Panel SSMIS QA Performance by latitude band. Scatter plots of the NFLUX SSMIS QA product performance and ship/buoy observations. The number of observations is listed in the upper left corner of each panel.

The performance of the NFLUX SSMIS Qa product based on zonal latitude bands is shown in Figure 3- 3. The combined SSMIS statistics associated with these zonal bands are shown in Table 6. In the latitude bands from ±15°, the effect of the 22 GHz high moisture corrections is evident. Within the 15° to 30° band (lower left panel) there is an asymptotic indication in the lower moisture levels. Further analysis indicates that the cluster of overly-moist data is associated with the East China Sea and the US coastal Gulf of Mexico during the winter months. Further analysis leading to improved performance will be accomplished in subsequent releases of NFLUX.

3.3.2 AMSU QA

The NFLUX AMSU Qa product performance is shown in Figure 3- 4, Figure 3- 5, Table 7, and Table 8. The global distribution of the quality-controlled 338623 observations with QC<90% (Figure 3- 4, upper left panel) indicates global coverage is good except for the extreme southern high latitudes. The bias distributions of both the NFLUX AMSU Qa and corresponding NOGAPS Qa (referenced to ship/buoy observations) are shown in the upper right panel of Figure 3- 4. The AMSU Qa bias is 70% less than the NOGAPS bias (i.e. -0.33 versus -1.06 g kg^{-1}). There is a 70% probability of NOGAPS underestimating the humidity at the ocean surface. The NFLUX

AMSU QA probability is much more Gaussian in shape, with a cumulative negative bias of 53%.

Table 6: SSMIS Qa Product Performance by Latitude. The SSMIS Qa product observations were divided into latitude bands to determine their specific performance by global regions. The bands were based on the density of the observations with the number of observations shown in the 6-panel presentation above.

Lat Band	ME	SD	RMSE	R^2
-90° to -15°				
NFLUX	-0.6959	1.7316	1.8662	0.8057
NOGAPS	-1.2893	1.6547	2.0976	0.8197
-15° to 0°				
NFLUX	0.1437	2.5332	2.5372	0.4966
NOGAPS	-1.5197	1.394	2.0622	0.6819
0° to 15°				
NFLUX	0.6761	2.7533	2.8351	0.3683
NOGAPS	-1.24	1.4325	1.8947	0.536
15° to 30°				
NFLUX	-0.5886	2.2655	2.3407	0.6526
NOGAPS	-1.2739	1.8359	2.2346	0.756
30° to 45°				
NFLUX	-0.3151	1.7419	1.7701	0.768
NOGAPS	-1.0405	1.7706	2.0536	0.7744
45° to 90°				
NFLUX	-0.0478	1.2785	1.2794	0.7144
NOGAPS	-0.5585	1.0828	1.2184	0.7643

Scatter plots of the NFLUX and NOGAPS match-ups to ship/buoy observations are shown in the lower figures of Figure 3- 4. As with the SSMIS comparison, distribution of the scatter is shown by relative colors, with the warmer colors indicating a greater concentration of data. There is a greater degree of symmetry for the distribution of NFLUX AMSU Qa (lower left panel) versus the ship/buoy observations, than in the distribution of NOGAPS (lower right panel) measured against the ship/buoy observations. NOGAPS also has a lower correlation coefficient (0.901) than the AMSU Qa (0.907). Evident in the distribution is the asymptotic behavior at higher moisture levels, with a practical limit of about 19 g kg^{-1} for NOGAPS, while the AMSU Qa demonstrates a better ability to measure the highest humidity levels.

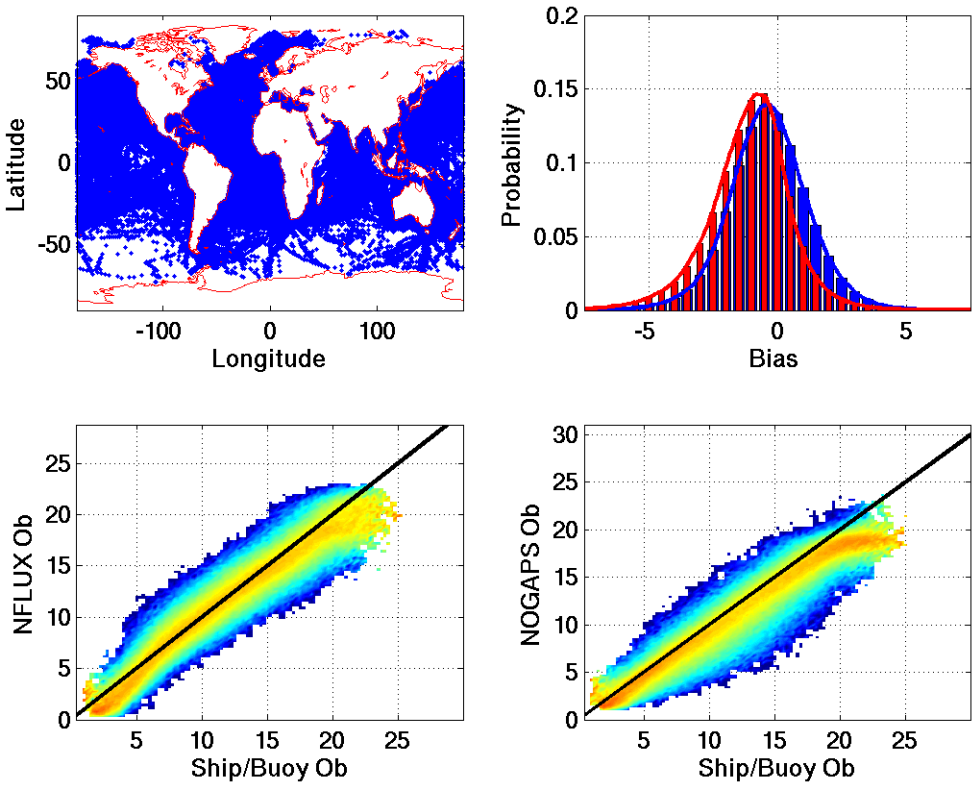

Figure 3- 4 4-Panel AMSU Qa Performance Summary. The upper left panel shows the distribution of the matched up observations. The upper right panel shows the distributions of NFLUX minus ship/buoy observation (blue) and of NOGAPS minus ship/buoy (red). The lower left shows a scatter plot of the NFLUX errors that has been shaded to show the relative distribution of the scatter. The increased scatter above the ship/buoy observation of 20 g kg^{-1} is due to the high-Qa correction based on a combination of the 52.8 and 53.6 GHz 22 channels. The thick black line shows a one-to-one correlation for visual reference. For comparison the NOGAPS scatter plot is shown in the lower right panel.

Table 7 shows the summary of the global performance of the NFLUX AMSU Qa and the matched-up NOGAPS Qa products. The NOGAPS performance is slightly different than shown in Table 5 because of the different orbital parameters for the DMSP and POES satellites, which results in slightly different match-up times. The performances of the individual AMSU sensors are also indicated.

The AMSU Qa algorithm performance as a function of latitude is shown in Figure 3- 5, with the associated statistics in Table 8. Throughout the latitude ranges, the biases for the AMSU Qa product are less than the NOGAPS bias, as is the case for the RMSE. The weakest performance occurs in the 0^{o} to 15^{o} latitude band, for both AMSU Qa and NOGAPS. This is attributed to the high humidity values observed in this latitude band. The strongest performance as measured by the correlation coefficient occurs in the Southern Hemisphere band, -90^{o} to -15^{o} latitude. The correlation coefficient for AMSU Qa is 0.86 and for NOGAPS it is 0.83. The 15^{o} to 30^{o} latitude band for the AMSU Qa product shows the 'S'-shape distribution over the range associated with over- (under-) prediction for low (high) *in situ* values. The over-estimation in moisture for the lower range shown is also evident in the SSMIS Qa product.

Table 7: AMSU Qa Product Performance. A total of 338623 match ups were generated from January 2010 through July 2012. The biases, standard deviations, and root mean square error estimates for the NFLUX product are compared to the NOGAPS values corresponding to the observation location and time of the satellite data. The individual satellite performance values are also indicated.

AMSU Qa				
	ME	**SD**	**RMSE**	**R^2**
NFLUX	-0.3307	1.5853	1.6194	0.9071
NOGAPS	-1.0617	1.6338	1.9485	0.9009
Satellites				
N15:	-0.4275	1.598	1.6542	0.9041
N18:	-0.2203	1.5881	1.6033	0.9044
N19:	-0.1303	1.607	1.6123	0.9047
N22:	-0.4898	1.5117	1.5891	0.9178

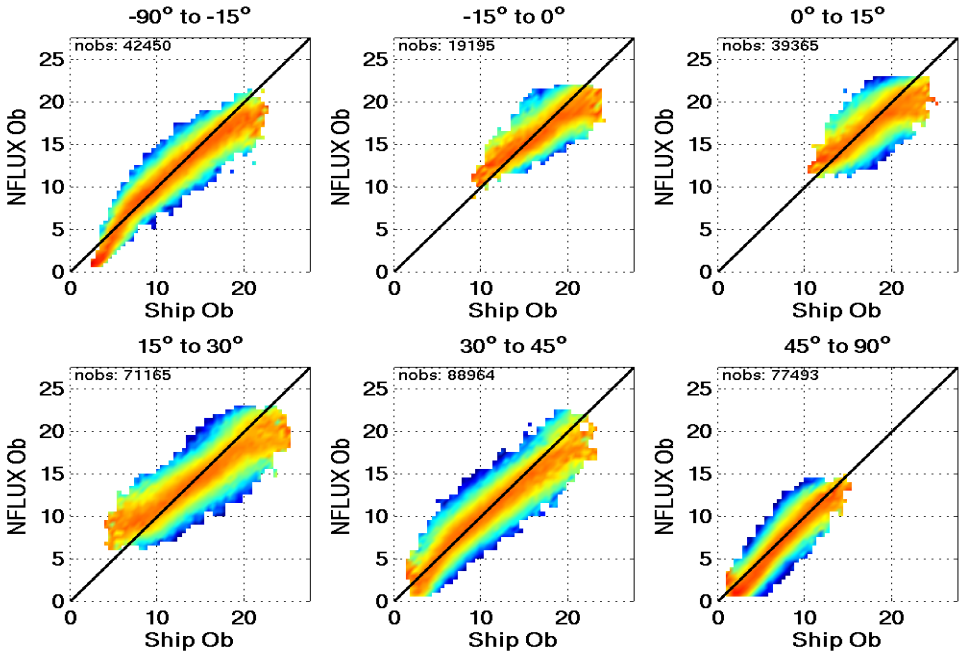

Figure 3- 5: 6-Panel AMSU Qa Performance by latitude band. Scatter plots of the NFLUX AMSU Qa product performance and ship/buoy observations. The number of observations is shown in the upper corner of each panel.

Table 8: AMSU Qa Product Performance by Latitude. The AMSU Qa product observations were divided into global bands to assess their performance by latitude. The bands were based on the density of the observations with the number of observations shown in the 6-panel presentation above.

Lat Band	ME	SD	RMSE	R^2
-90° to -15°				
NFLUX	-0.3352	1.5167	1.5533	0.8599
NOGAPS	-1.3092	1.6807	2.1304	0.8284
-15° to 0°				
NFLUX	-0.4952	1.5905	1.6657	0.5905
NOGAPS	-1.524	1.4032	2.0715	0.674
0° to 15°				
NFLUX	-0.5009	1.6282	1.7035	0.4558
NOGAPS	-1.2672	1.424	1.9062	0.5341
15° to 30°				
NFLUX	-0.3915	1.8846	1.9248	0.715
NOGAPS	-1.2905	1.8423	2.2493	0.7499
30° to 45°				
NFLUX	-0.1022	1.5806	1.5839	0.8062
NOGAPS	-1.0435	1.8153	2.0938	0.7659
45° to 90°				
NFLUX	-0.4076	1.2363	1.3017	0.7906
NOGAPS	-0.5179	1.1167	1.231	0.754

3.3.3 AMSU Ta

The NFLUX AMSU Ta product performance is shown in Figure 3- 6, Table 9, Figure 3-7, and Table 10. The distribution of the quality-controlled 386777 observations with QC<90% (Figure 3- 6, upper left panel) indicates good global coverage. The bias distributions of both the NFLUX AMSU Ta and corresponding NOGAPS Ta measured against matched ship/buoy observations are shown in the upper right panel of Figure 3-6. The AMSU Ta bias is 15% larger than the NOGAPS bias (i.e. -0.25 versus -0.21 °C), though it should be noted that the percentage difference is high due in part to the low mean bias of both products. Both products demonstrate a strongly Gaussian performance. The NFLUX AMSU Ta cumulative negative bias is 52%, while the NOGAPS cumulative negative bias is 46%.

Scatter plots of the NFLUX and NOGAPS match-ups to ship/buoy observations are shown in the lower figures of Figure 3- 6. As with the prior comparisons, distribution of the scatter is shown by relative colors, with the warmer colors indicating a greater concentration of data. The performance of the NFLUX AMSU Ta product is essentially equal to the NOGAPS Ta performance. The correlation coefficient for NFLUX Ta is 0.957 while NOGAPS is 0.958. The RMSE for NFLUX is 0.02°C greater than that for NOGAPS.

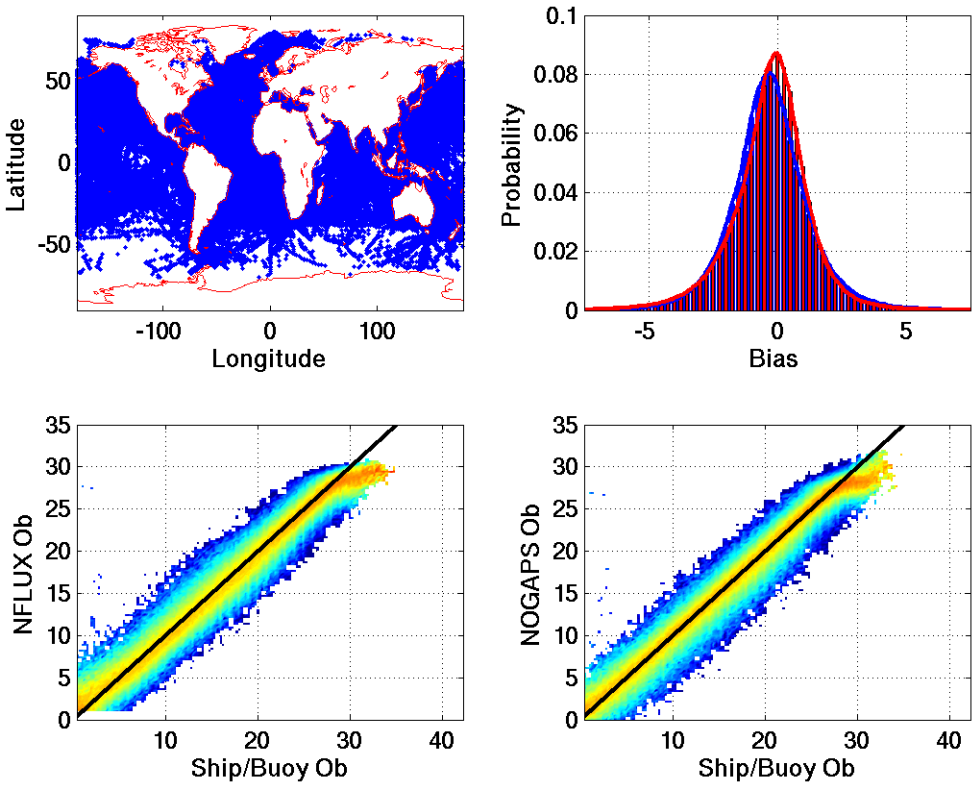

Figure 3- 6: 4-Panel AMSU Ta Performance Summary. The upper left panel shows the distribution of the matched up observations. The upper right panel shows the distribution of NFLUX minus ship/buoy observation (blue) compared to the distribution for NOGAPS (red). The lower left shows a scatter plot for NFLUX Ta and for comparison the NOGAPS scatter plot is shown in the lower right panel.

Table 9 shows the summary of the global performance of the NFLUX AMSU Ta and the matched up NOGAPS Ta products. The performances of the individual AMSU sensors are also indicated.

The NFLUX Ta algorithm performance as a function of latitude is shown in Table 10 and in Figure 3- 7. In the low latitude bands of -15° to 0° and 0° to 15°, the NFLUX Ta algorithm demonstrates low bias, slightly less than 0.1°C, along with a lower RMSE error and nearly equivalent correlation coefficients to those of NOGAPS. In the Southern Hemisphere, the bias is lower for NOGAPS Ta (-0.12°C versus -0.28°C), but the scatter of the data is higher for NOGAPS (1.35°C versus 1.33°C); see Table 10. This is due in part to the slightly better performance of the NFLUX Ta product at higher observation values.

Table 9: AMSU Ta Product Performance. A total of 386777 match ups were generated from January 2010 through July 2012. The biases and the standard deviations are combined into a single root mean square (RMSE) error estimate for the NFLUX product and compared to the NOGAPS values associated with the observation location and time of the satellite data. The individual satellite performance values are also shown.

AMSU Ta				
	ME	**SD**	**RMSE**	**R^2**
NFLUX	-0.2542	1.6398	1.6594	0.9574
NOGAPS	-0.2147	1.6259	1.64	0.9582
Satellites				
N15:	-0.229	1.6677	1.6833	0.9553
N18:	-0.2709	1.62	1.6425	0.9563
N19:	-0.2153	1.6012	1.6156	0.9583
N22:	-0.3092	1.6531	1.6818	0.9593

Table 10: AMSU Ta Product Performance by Latitude. The AMSU Ta product observations were divided into latitude bands to determine their specific performance by global regions. The bands were based on the density of the observations with the number of observations shown in the 6-panel presentation above.

Lat Band	**ME**	**SD**	**RMSE**	**R^2**
-90^o to -15^o				
NFLUX	-0.2848	1.334	1.364	0.9516
NOGAPS	-0.1189	1.3507	1.3559	0.9504
-15^o to 0^o				
NFLUX	-0.13	1.1213	1.1288	0.7491
NOGAPS	-0.2412	1.1249	1.1505	0.7474
0^o to 15^o				
NFLUX	-0.2428	1.5021	1.5216	0.3972
NOGAPS	-0.3131	1.5029	1.5352	0.3898
15^o to 30^o				
NFLUX	-0.2651	1.5136	1.5367	0.8259
NOGAPS	-0.2038	1.4915	1.5053	0.833
30^o to 45^o				
NFLUX	-0.344	2.0381	2.067	0.8745
NOGAPS	-0.2738	1.9909	2.0097	0.8833
45^o to 90^o				
NFLUX	-0.1638	1.5617	1.5703	0.8689
NOGAPS	-0.1425	1.5801	1.5865	0.8687

Globally, at a ship/buoy observation of $30^oC \pm 0.25^oC$, NFLUX Ta has a bias of -1.79^oC and NOGAPS has a bias of -1.99^oC. Comparison between these high values of Ta in Figure 3- 7 and Figure 3- 8 shows a distinct nonlinearity in the NOGAPS data with a distinct 'S'-shaped distribution in the 0^o to15^o latitude panel (Figure 3- 8, upper right panel). This artifact is more asymptotic in the NFLUX Ta product. Both NFLUX and NOGAPS show degradation in performance in the 15^o-30^o bands. NFLUX shows a marked asymptotic behavior below 15^oC, lower left panel of Figure 3- 7. Also evident is the slight decrease in the NOGAPS correlation below 15^oC.

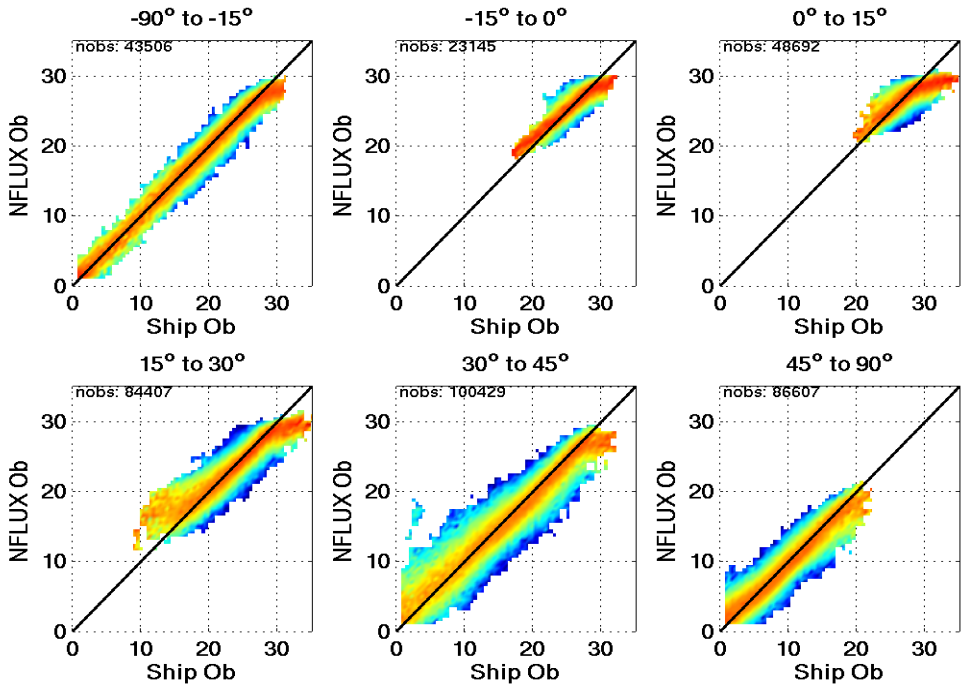

Figure 3- 7: 6-Panel AMSU Ta Performance by latitude band. Scatter plots of the NFLUX AMSU Ta product performance and ship/buoy observations. The number of observations is shown in the upper corner of each panel.

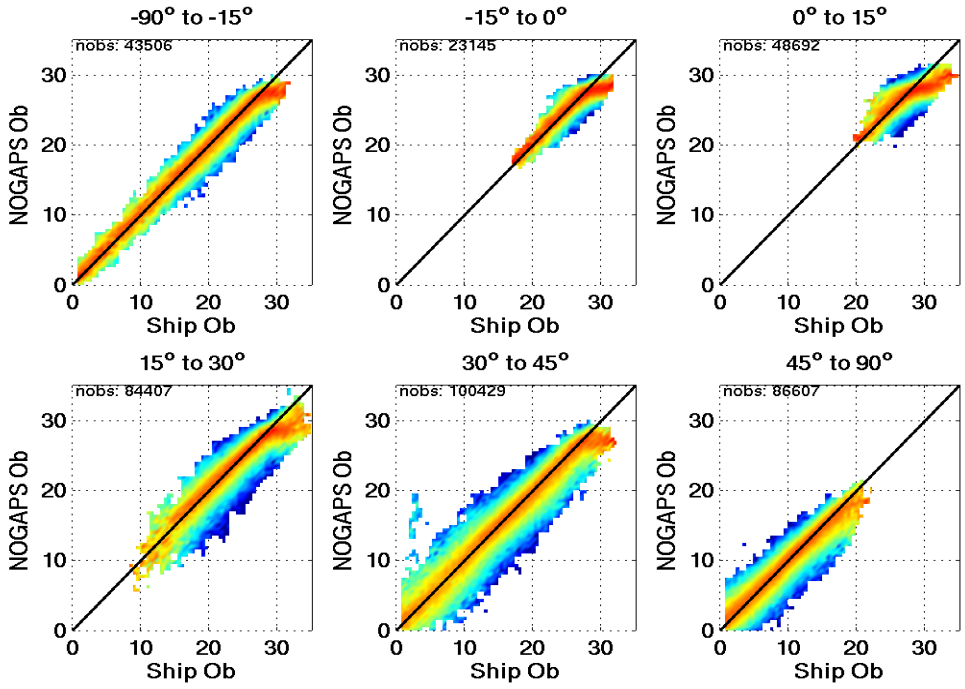

Figure 3- 8: 6-Panel NOGAPS Ta Performance by latitude band. Scatter plots of the NOGAPS Ta product performance and ship/buoy observations. Of note is the 'S' –shaped distribution in the higher values for Ta, mostly noticeable in the 0^0 to 15^0 latitude.

3.3.4 SSMIS U10

The NFLUX SSMIS U10 product performance is shown in Figure 3- 9,

Table 11, Figure 3- 10, and Table 12. The global distribution of the 136952 observations is shown in Figure 3- 9, upper left panel. The bias distributions of both the NFLUX SSMIS U10 and corresponding NOGAPS U10 to ship/buoy observations are shown in the upper right panel of Figure 3- 9. Table 11 provides the global statistics for the wind speed products. These are different from the prior statistics in the sense that the NFLUX SSMIS U10 bias is positive 0.62 m s^{-1}, while the NOGAPS bias is -0.47 m s^{-1}. The bias difference is over 1 m s^{-1}. The cumulative probability for underestimating the wind speed for NFLUX is 37%, while the NOGAPS probability is 54%.

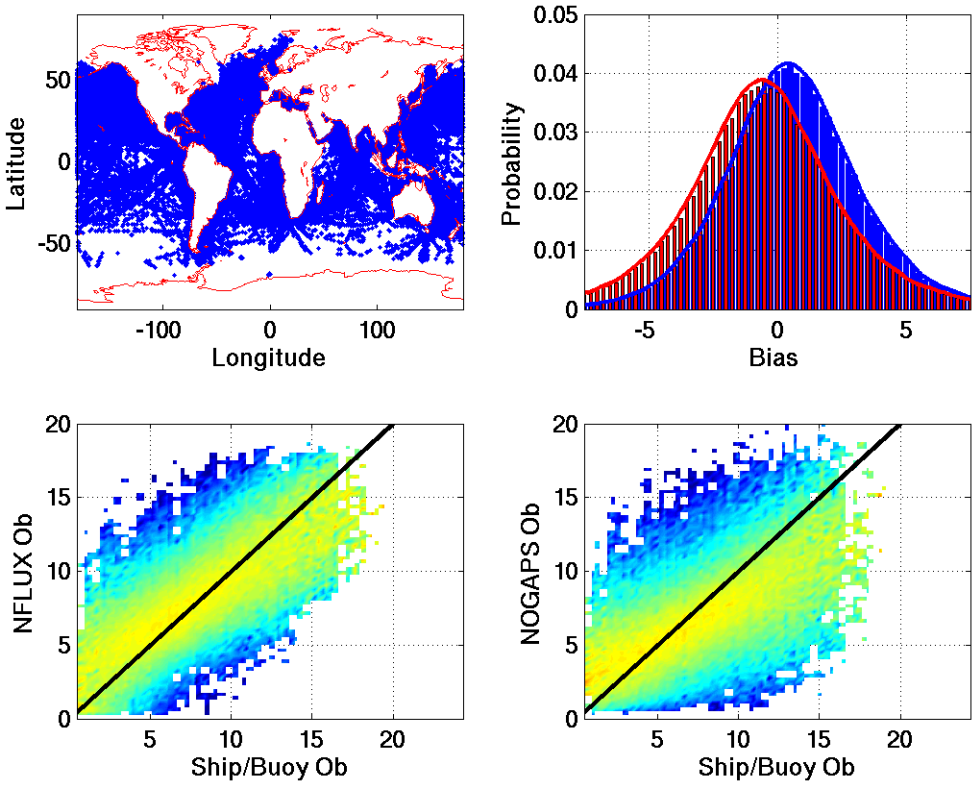

Figure 3- 9: 4-Panel SSMIS U10 Performance Summary. The upper left panel shows the distribution of the matched up observations. The upper right panel shows the distributions of NFLUX minus ship/buoy observation (blue) and of NOGAPS minus ship/buoy observation (red). The lower right shows the NFLUX scatter plot with the NOGAPS scatter plot shown in the lower right panel.

Scatter plots of the NFLUX and NOGAPS matchups to ship/buoy observations are shown in the lower figures of Figure 3- 9. The distribution of the scatter is shown by relative colors, with the warmer colors indicating a greater concentration of data. The NFLUX U10 (lower left panel) performance shows a much lower correlation than the other NFLUX products, i.e. 0.43, but a greater correlation than NOGAPS wind speed at 0.28. The higher probability for an underestimated wind speed is clearly evident in the

NOGAPS distribution (lower right panel). In a very low wind speed regime, less than 5 m s^{-1}, NOGAPS has bias of 1.6 m s^{-1}, while NFLUX has a greater bias of 2.1 m s^{-1}. Overall, the scatter of the NFLUX U10 product is less than that associated with the NOGAPS U10, leading to an RMSE of 2.8 m s^{-1} for NFLUX and 3.2 m s^{-1} for NOGAPS. The performances of the individual SSMIS sensors are also indicated in Table 11.

Table 11: SSMIS U10 Product Performance. A total of 136952 match ups were generated from January 2010 through July 2012. The biases and the standard deviations are combined into a single root mean square (RMSE) error estimate for the NFLUX product and compared to the NOGAPS values associated with the observation location and time of the satellite data. The individual satellite performance values are also indicated.

SSMIS U10				
	ME	**SD**	**RMSE**	**R^2**
NFLUX	0.6234	2.7555	2.8251	0.4296
NOGAPS	-0.4749	3.1753	3.2106	0.2815
Satellites				
F16:	0.5002	2.7144	2.7601	0.4292
F17:	0.3498	2.6908	2.7134	0.4323
F18:	0.9043	2.8058	2.9479	0.4309

Table 12: SSMIS U10 Product Performance by Latitude. The SSMIS U10 product observations were divided into latitude bands to determine their specific performance by global regions. The bands were based on the density of the observations with the number of observations shown in the 6-panel presentation above.

Lat Band	**ME**	**SD**	**RMSE**	**R^2**
-90° to -15°				
NFLUX	0.2841	2.6822	2.6971	0.3473
NOGAPS	-0.5666	2.8748	2.93	0.2478
-15° to 0°				
NFLUX	0.4294	2.3212	2.3604	0.2527
NOGAPS	-0.6904	2.1319	2.2408	0.2755
0° to 15°				
NFLUX	0.4745	2.4638	2.509	0.3958
NOGAPS	-0.6883	2.316	2.4161	0.4098
15° to 30°				
NFLUX	0.3562	2.419	2.4451	0.4044
NOGAPS	-0.5981	2.6299	2.697	0.2746
30° to 45°				
NFLUX	0.7716	2.9521	3.0512	0.4046
NOGAPS	-0.3706	3.6678	3.6864	0.2046
45° to 90°				
NFLUX	1.0996	3.1209	3.3089	0.3899
NOGAPS	-0.2077	3.9047	3.9102	0.1992

The performance of the NFLUX SSMIS U10 product based upon zonal bands is shown in Figure 3- 10. The statistics associated with these zonal bands are shown in Table 12. In the latitude bands from ±15° the NFLUX product has a lower ME but a significantly higher RMSE. This difference is well within the precision estimate in section 3.2, Table

3. The regions outside the equatorial bands demonstrate that the performance of the NFLUX U10 algorithm represents an improvement over the NOGAPS U10 product. Figure 3- 10 shows the colored scatters plots for the NOGAPS U10 product as a function of latitude band.

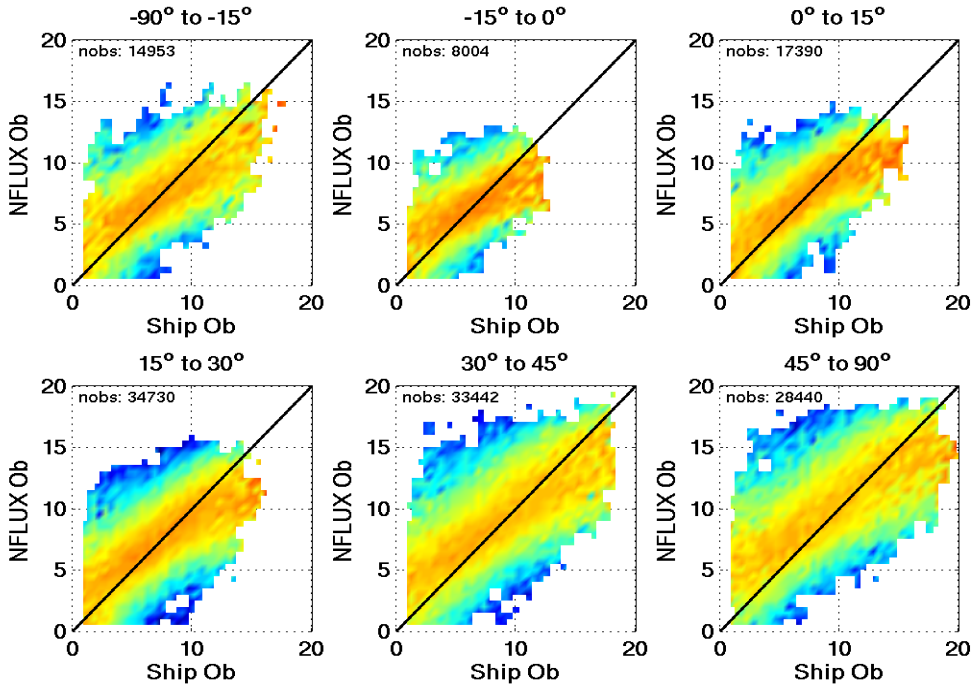

Figure 3- 10: 6-Panel SSMIS U10 Performance by latitude band. Scatter plots of the NFLUX SSMIS U10 product performance and ship/buoy observations. The number of observations is shown in the upper corner of each panel.

3.3.5 WindSat U10

The WindSat data is obtained as a georeferenced EDR. It is available in three resolution levels: high, medium, and low. The high resolution is produced in an approximate 12.5 by 12.5 km grid, the medium is at a 35 by 53 km resolution, and the low is at a 50 by 71 km resolution. The high and low resolutions were compared with the ship observed database of wind speeds. The low resolution was selected for use based upon the reduced RMSE value and the improved correlation, as shown in Table 13.

Table 13: WindSat High and Low Resolution performance comparisons. The WindSat data was matched-up to the ship/buoy observations from January 2010 through July 2012. The Low Resolution dataset was selected to be incorporated into the NFLUX system.

	ME	SD	RMSE	R^2
High Resolution	0.6717	2.4656	2.5554	0.4884
Low Resolution	0.7196	2.3929	2.4988	0.5084

The WindSat U10 product performance is shown in Figure 3-11, Table 14, Figure 3-12, Figure 3-13, and Table 15. As above, the global distribution of the 100596 observations and their biases are shown in the upper panels of Figure 3-11. The global statistics for the wind speed products are shown in Table 14. Note that the NFLUX U10 product statistics are included for comparison purposes. Similar to NFLUX, the WindSat bias is between 0.5 and 1.0 m s^{-1}. The NOGAPS wind speed bias for observation times associated with WindSat is slightly positive at 0.19 m s^{-1}. The correlation coefficient for the WindSat sensor is 0.51, which is greater than the 0.41 value for NOGAPS. This value for NOGAPS is greater than what was calculated for the DMSP/SSMIS match up time periods where the correlation coefficient was 0.28. One possible explanation for the differences between the correlation coefficients found for the NFLUX/NOGAPS and WindSat/NOGAPS match ups is the time of observation. Figure 3-13 shows the differences between the match up times for the two satellite types.

Table 14: WindSat U10 Product Performance. A total of 100596 match ups were generated from January 2010 through July 2012. The biases and the standard deviations are combined into a single root mean square (RMSE) error estimate for the WindSat product and compared to the NOGAPS values associated with the observation location and time of the satellite data. The NFLUX U10 product performance is repeated for comparison purposes.

WindSat				
	ME	**SD**	**RMSE**	**R^2**
WindSat	0.7196	2.3929	2.4988	0.5084
NOGAPS	0.1925	2.664	2.6709	0.4057
NFLUX	0.6234	2.7555	2.8251	0.4296

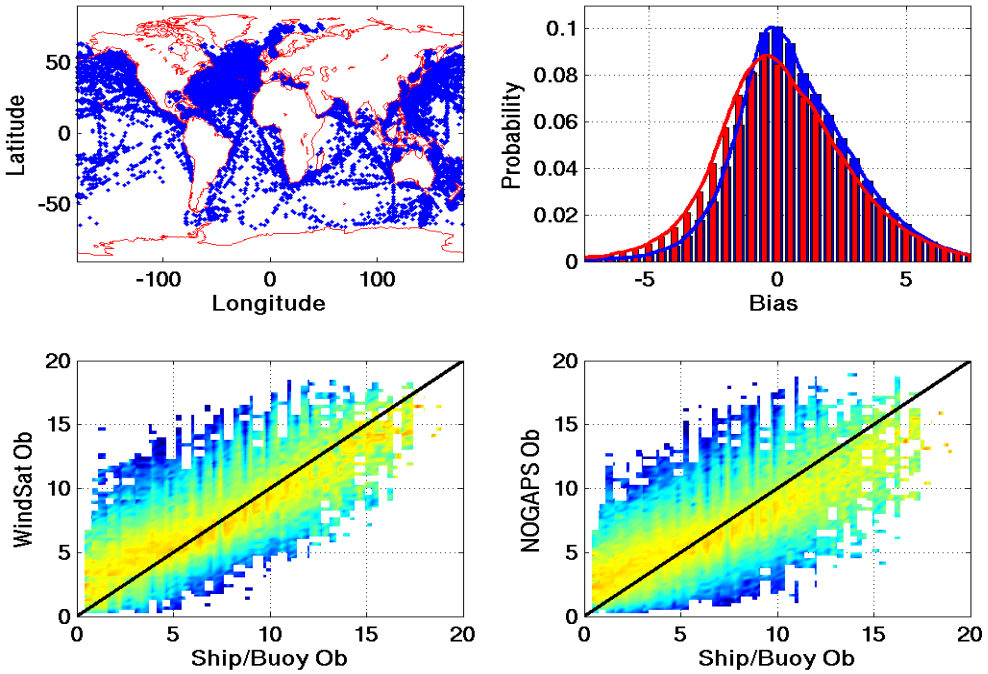

Figure 3-11: 4-Panel WindSat U10 Performance Summary. The upper left panel shows the distribution of the matched up of the 100596 observations. The upper right panel shows the distributions of WindSat minus ship/buoy observation (blue) and of NOGAPS minus ship/buoy observation (red). The WindSat scatter plot (lower left) is compared to the NOGAPS scatter plot is shown in the lower right panel.

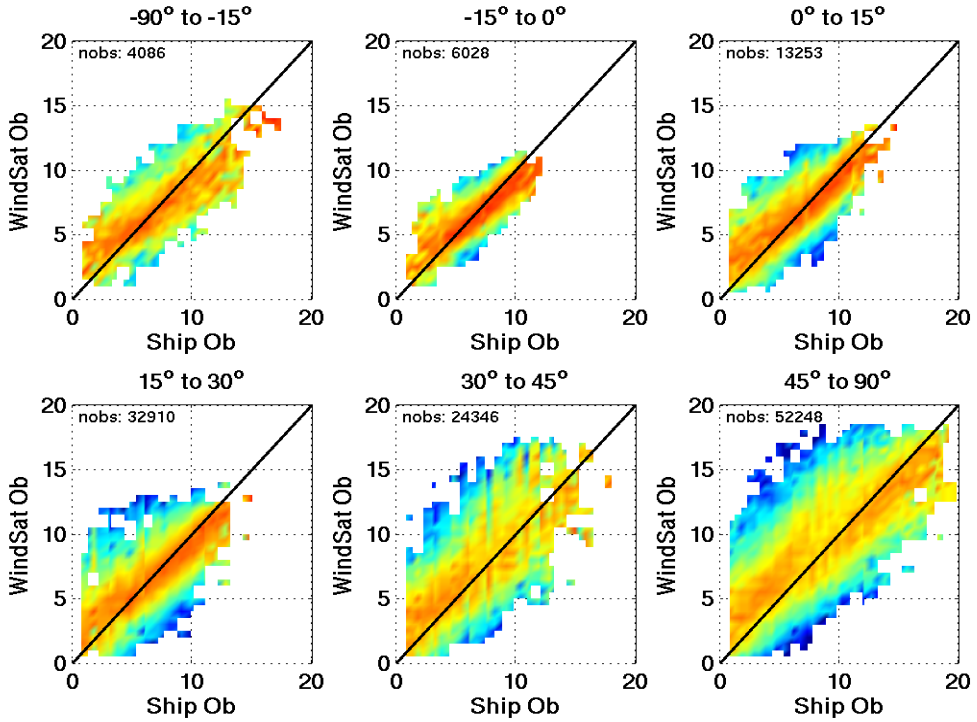

Figure 3-12: 6-Panel WindSat U10 Performance by latitude band.

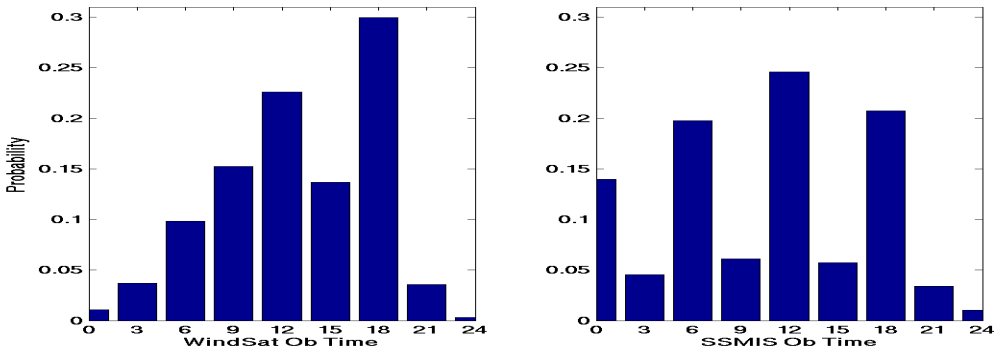

Figure 3-13: Observations Times for WindSat and SSMIS. The observations for the two satellites match up databases are compared. The NOGAPS U10 product performance is more robust during the periods associated with the WindSat matchup at R^2=0.41, while the SSMIS matchup time periods results in an R^2=0.28.

Table 15: WindSat U10 Product Performance by Latitude. The WindSat U10 product observations were divided into latitude bands to determine their specific performance by global regions.

Lat Band	ME	SD	RMSE	R^2
-90° to -15°				
WINDSAT	-0.1111	2.207	2.2095	0.5324
NOGAPS	-0.5675	2.3717	2.4383	0.4757
-15° to 0°				
WINDSAT	-0.1447	1.3731	1.3806	0.5487
NOGAPS	-0.881	1.518	1.755	0.4447
0° to 15°				
WINDSAT	0.2471	1.6433	1.6617	0.5657
NOGAPS	-0.6276	1.7658	1.8739	0.4953
15° to 30°				
WINDSAT	0.2096	1.9176	1.929	0.5541
NOGAPS	-0.1978	2.0307	2.0403	0.4925
30° to 45°				
WINDSAT	0.8468	2.5455	2.6826	0.504
NOGAPS	0.7552	3.0499	3.142	0.3351
45° to 90°				
WINDSAT	1.295	2.6919	2.9872	0.5058
NOGAPS	0.6885	2.993	3.0711	0.4191

4 Discussion

The direct assimilation of satellite-based surface observations into an operational ocean model is the underlying purpose and goal of this work. The early decision to focus on passive microwave sensors provided key surface measurements of specific humidity, air temperature, and scalar wind speed. The goal of the NFLUX system is to provide high quality data within the operational cycle of U.S. Navy ocean modeling. The initial sets of algorithms were based on those found in literature (Jackson et al., 2006 and Goodberlet et al., 1989). In order to achieve the desirable error characteristics for each of the NFLUX products, unique algorithms for each satellite/sensor/product combination were needed.

Figure 4- 1 shows the global distribution of the *in situ* observations utilized to develop the unique algorithms from January 2010 to January 2012. Experience demonstrated that this multi-year dataset was sufficient to develop the global algorithms.

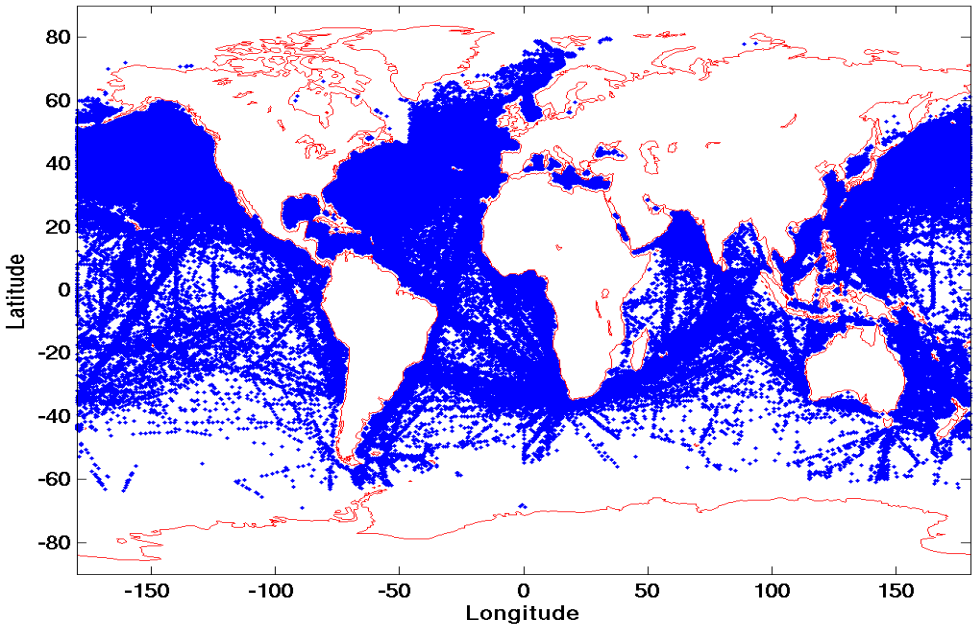

Figure 4- 1: Global distribution of the *in situ* observation data set. Data was collected from ships with identifiable call signs and buoys where the height of observation was known.

The two different passive microwave sensors onboard the POES/METOP and DMSP satellites use different frequencies and polarizations, as shown in Table 16. Figure 4- 2 and Figure 4- 3 show the atmospheric weighting functions for each of the passive microwave channels on the AMSU and SSMIS sensors. The weighting functions indicate where the primary information is being extracted as a function of altitude. The NFLUX channels used are a subset of these shown. Both the AMSU and the SSMIS NFLUX algorithms utilize channels that have the peak of the weighting function above

the surface, 53.6 GHz and 183.3 ± 3 GHz respectively. This near-surface information was found to improve the performance of the algorithms.

Table 16: AMSU and SSMIS Channels used. The channels used by the two passive microwave sensors are very different in both their frequencies and polarizations. The AMSU is used to produce Qa and Ta NFLUX products. The SSMIS is used to produce Qa and U10 NFLUX products. The channels used for Imager-only algorithm and Imager/Sounder algorithms are shown. *The 91GHz SSMIS channels are only produced on odd number scans. **The 183.3 GHz channel is interpolated to the FOVs of the other channels.

AMSU Channel Number	AMSU Freq (GHz)	SSMIS Channel Number	SSMIS Freq (GHz)	Imager Only Algorithm	Imager + Sounder Algorithm
1	23.8	10	183.31+/-3**	X	X
2	31.4	12	19.35 H	X	X
3	50.3	13	19.35 V	X	X
4	52.8	14	22.235 V	X	X
5	53.6	15	37 H	X	X
15	89	16	37 V		X
		17	91.655 V*		X
		18	91.655H*		X

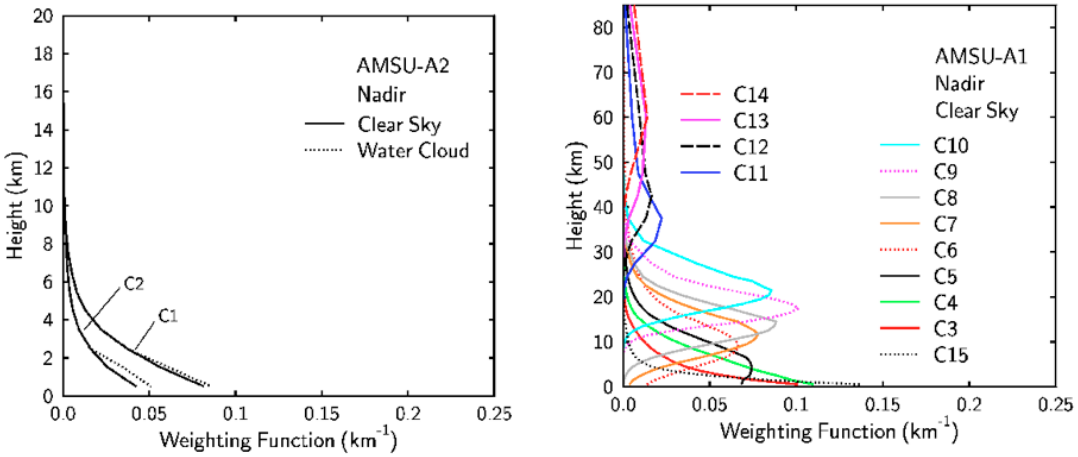

Figure 4- 2: AMSU Weighting Functions. As in Figure 4- 3 except for AMSU channels. The channel numbers correspond to those listed in Table 16. The channel numbers indicated correspond to those in Table 16 (http:;;http://amsu.cira.colostate.edu/weights.html, accessed 23JAN2013).

Table 16 shows that there are two possible sets of algorithms for each satellite that use satellite-only information. These were classified as either "imager-only" or "imager/sounder" to distinguish them. In practice, the AMSU produces primarily the combined imager/sound products and only the SSMIS produces both. The channels that are on the sounder-portion of the sensor are only produced for odd-numbered scans. The reader interpolates the 183.3 brightness temperature to the location of the imager FOV's.

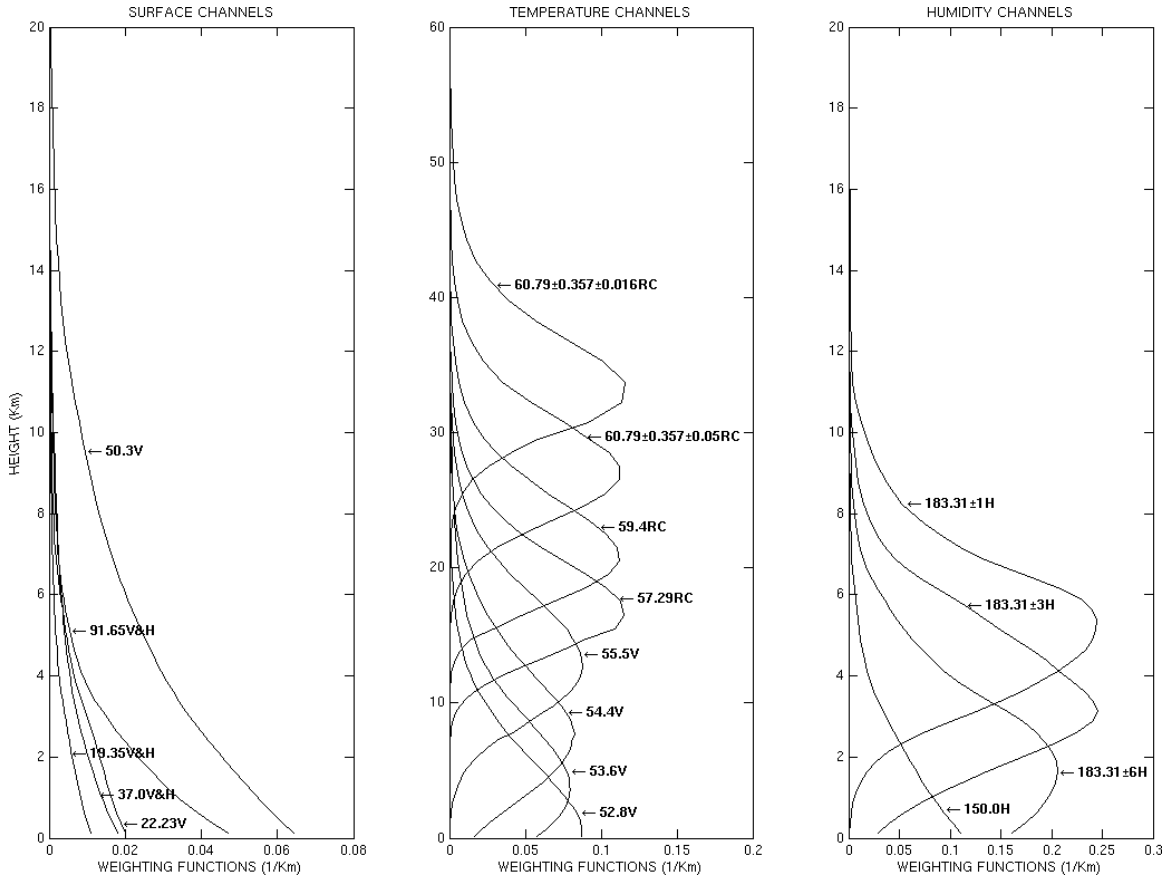

Figure 4- 3: SSMIS Channel Weighting Functions. Passive microwave channels response to different regions within the atmosphere as a function of their frequency (Karbuo, F, P. Bauer, A. Geer, W. Bell, SAF-Hydrology Final Report).

A 4 x 4 matrix of 183.3 brightness temperatures is used to interpolate. No unique interpolation of the 91 GHz channels is necessary because they are provided already remapped. If some of the FOV's within the 4 x 4 matrix are missing due to proximity of the scan edge to land or clouds, no remapping is done and the imager-only algorithm is utilized.

An improved metric to compare NFLUX and NOGAPS to the matched up *in situ* observations, skill score, is used (Murphy, 1988 and 1995). The skill score is shown in equation (8) below. It is composed of three constituents: the correlation coefficient, the conditional bias, and the unconditional (systematic) bias.

$$SS(f,x) = r_{fx}^2 - \left[r_{fx} - \left(s_f / s_x \right) \right]^2 - \left[\left(\overline{f} - \overline{x} \right) / s_x \right]^2, \qquad (8)$$

where f is the *in situ* observation, x is either the NFLUX or NOGAPS observation, r_{fx} is the correlation coefficient between the *in situ* and NFLUX/NOGAPS data set, s_f and s_x are the standard deviations of the *in situ* and NFLUX/NOGAPS data sets, and the overbars indicate a mean of the data sets.

The second term will vanish if the slope of the regression line is unity; otherwise the effect of this term is to decrease the overall skill score (Murphy, 1988). The second term componets are $r_{fx} \sim 0.9$ and $(s_f/s_x) \sim 1.02$. The difference between the components of the second term is O(0.1). Therefore this term would have a very small impact on modifying the skill score from the primary component of the regression coefficient.

The third term vanishes if the mean of the NFLUX (NOGAPS) population is equal to the mean of the *in situ* observations. If the mean of the NFLUX population is simply modeled as the *in situ* mean modified by the systematic bias (δ) then:

$$\left[\left(\overline{f} - \left(\overline{f} + \delta \right) \right) \Big/ s_x \right]^2 \longrightarrow \left(-\delta / s_x \right)^2 . \tag{9}$$

The NFLUX/NOGAPS δ can be characterized as O(1) or less. In general NFLUX/ NOGAPS variance can be characterized as O(10), so the ratio of the terms is ~1/3.. Therefore the third term will tend to have an impact on the final skill score of O(0.1).

The two-year match up database allowed a simple bootstrapping technique to be employed to estimate the confidence limits around the skill score. This was necessary because the skill score is a linear combination of several different representations of the data. The match up data set was randomly subsampled at the 10% level. These realizations were repeated to provide a robust sample of the skill scores. The probability of the skill scores was estimated directly with a histogram and the 2.5% and 97.5% levels in the probability distribution function was estimated to form the confidence limits around the peak of the histogram of the skill scores.

4.1 Specific Humidity

The NFLUX biases are presented globally in Figure 4- 4. Data from January 2010 through July 2012 was averaged into 1.25^o bins. The size of the square bias marker is proportional to the number of observations in each 1.25^o bin and is a proxy for the confidence of the bin bias. The figure indicates that the mid-latitudes of the ocean basins are well modeled with a slight dry bias. This was noted in the panels in Figure 3-3. The western Pacific and extreme eastern Pacific tropical zones show distinct wet biases. The Arabian Sea shows a strong dry bias. These regional issues will be addressed later in this report. At the 95% confidence level (CL), NFLUX is a better estimator of the ocean surface Qa than is NOGAPS, as shown in Figure 4- 5. There is a global dry bias to this NOGAPS product with a slight tendency towards a zero bias only in the northern portions of the northern hemisphere ocean basins. This conclusion is supported by the histograms and colored scatter plots in Figure 3- 2. Table 17 compares the performance of both NOGAPS and NFLUX Qa products.

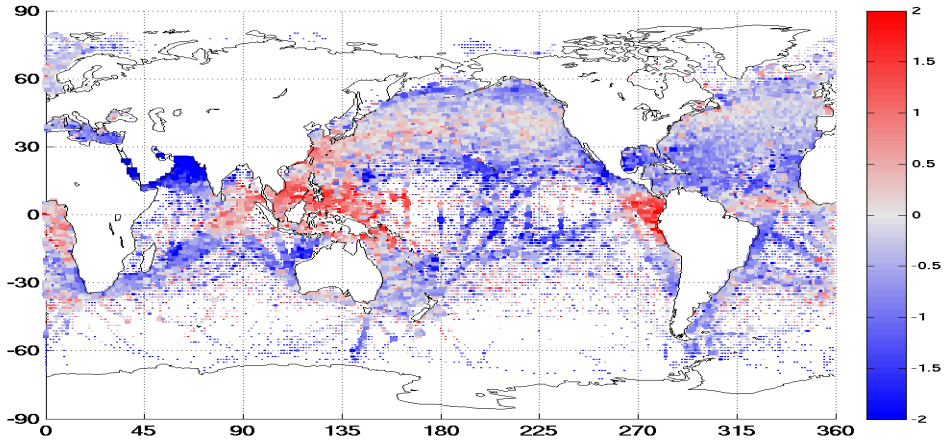

Figure 4- 4: NFLUX Average Global Biases. The average difference between the NFLUX observation and the corresponding *in situ* observation for the period of January 2010 through July 2012 is shown.

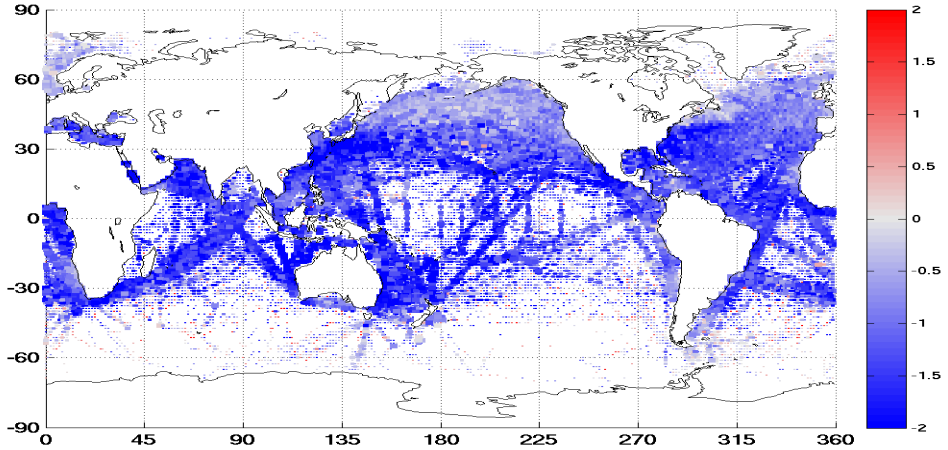

Figure 4- 5: NOGAPS Global Qa Bias. Similar to Figure 4- 4.

Table 17: Global Qa Skill Scores. The skill score using Murphy (1988) is shown along with a bootstrapped estimation of the 95% confidence limits (CL). The NFLUX system has better skill at estimating Qa than NOGAPS at the 95% confidence level.

Qa	95% Lower CL	Skill Score	95% Upper CL
NFLUX	0.8784	0.8824	0.8863
NOGAPS	0.8563	0.8608	0.8660

It is evident that the NOGAPS global Qa performance is not as good as the NFLUX Qa product at the 95% confidence limits based upon Table 5, Table 7, and Table 17. The NFLUX ME and RMSE are below those of NOGAPS. The overall impact on ocean model performance will be addressed in another validation report. However, it is worth noting that errors in specific humidity are directly proportional to errors in the latent heat

flux. The spatial and temporal evolution of the upper ocean is, in part, controlled by the latent heat flux.

The bulk formulation for latent heat flux content of the ocean is defined as:

$$LE = \rho L_E C_L U\left(Q_S - Q_A\right) \tag{10}$$

where ρ is the air density, L_E is the latent heat of evaporation, C_L is the latent heat transfer coefficient, U is the horizontal wind speed, Q_s is the saturation specific humidity at the sea surface, and Q_A is the specific humidity of the air. Using the years of match up data, the combined AMSU and SSMIS mean global NFLUX bias is -0.3068 g kg^{-1} with a mean NOGAPS bias of -1.070 g kg^{-1}. The average Qa for the *in situ* observations for this time period is 12.22 g kg^{-1}. The NOGAPS mean bias equates to an 8.8% global overestimation of latent heat over time. Equivalently, NFLUX Qa mean bias equates to a 2.5% latent heat overestimation.

4.2 Surface Air Temperature

The differences between the Ta products are not as large as for the Qa products. Figure 4- 6 shows the global bias for the NFLUX Ta product. The patterns are dissimilar to the NFLUX Qa global average in Figure 4- 4. The tight coupling between the Ta and the sea surface temperature is evident. Most notable is the general cool bias for the central northern Pacific basin, with the exception of the Gulf Stream area. The global NFLUX Ta skill score is shown in Table 18. The skill score for the northern Pacific basin is reduced to 0.9043 for NFLUX and 0.9114 for NOGAPS. These are equivalent at the 95% CL.

Table 18: Global Ta Skill Score. The skill scores for NFLUX and NOGAPS and the 95% CLs are shown. The performance of NFLUX is equivalent to NOGAPS at the 95% CL.

Ta	95% Lower CL	Skill Score	95% Upper CL
NFLUX	0.9530	0.9568	0.9604
NOGAPS	0.9531	0.9565	0.9607

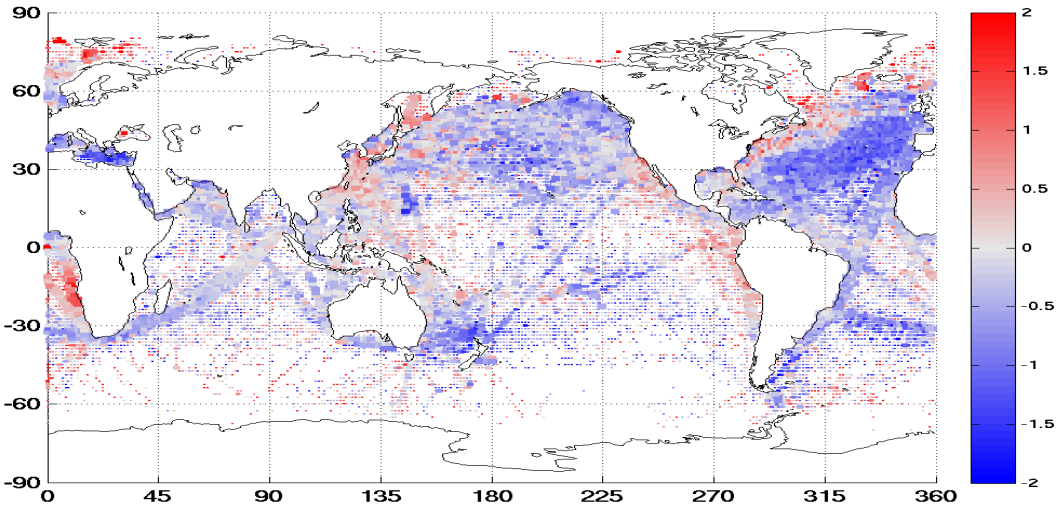

Figure 4- 6: Global NFLUX Ta Bias. As in Figure 4- 4, the NFLUX observation bias was averaged using 1.25° grid squares over a two-year period.

The pattern for the NOGAPS Ta product is shown in Figure 4- 7. Visually there appears to be a trend of the NOGAPS Ta values to be cooler than the *in situ* values for the western pacific basin and the Arabian Sea. Using the data from 20° to 60° latitude and 310° to 360° longitude, the ME bias for this large region is -0.20°C, with an RMSE of 1.70. This is contrast with the NFLUX Ta ME for this region of -0.53°C and an RMSE of 1.79. However, as noted above their skill scores are equivalent at the 95% CL.

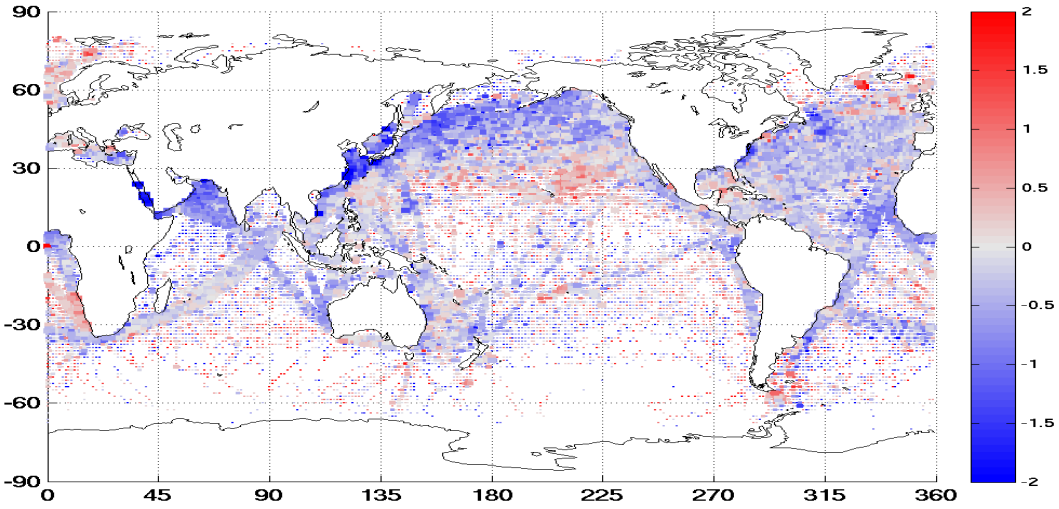

Figure 4- 7: Global NOGAPS TA Bias.

Similar to the relationship between the latent heat flux and Qa, the sensible heat flux and surface air temperature are related by:

$$SH = \rho C_p C_S U(T_a - SST) \tag{11}$$

where C_P is the specific heat capacity of the air, C_S is the sensible heat transfer coefficient, and T_a is the air temperature. As with Qa, a 5% error in Ta can be expected to produce a proportional error in the surface sensible heat flux.

4.3 Surface Wind Speed

Two separate processes provide surface wind speeds. Scalar wind speeds are produced from the SSMIS sensor on DMSPs F16, F17, and F18 using algorithms developed specifically for the NFLUX system. Also included in the NFLUX system are wind speeds calculated from the WindSat Environmental Data Record.

4.3.1 SSMIS Wind Speed

The global distribution of the bin-averaged scalar wind speed is shown in Figure 4- 8. The positive bias is supported by the histogram in Figure 3- 9. Figure 4- 9 shows the scalar wind speed calculated from the horizontal components generated by NOGAPS. The global skill score is 0.0808. The global bias for the NOGAPS wind speed is -0.48 m s^{-1}, whereas the NFLUX bias was 0.62 m s^{-1}.

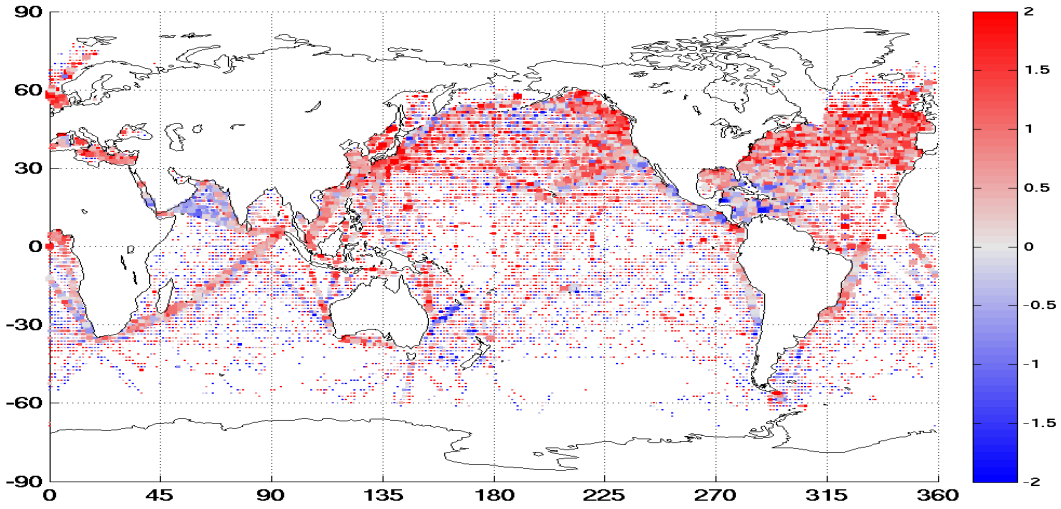

Figure 4- 8: NFLUX Scalar Wind Speed Bias. The NFLUX global bias is positive 59% of the time for the matched up observations and has a mean bias of 0.67 m s^{-1}.

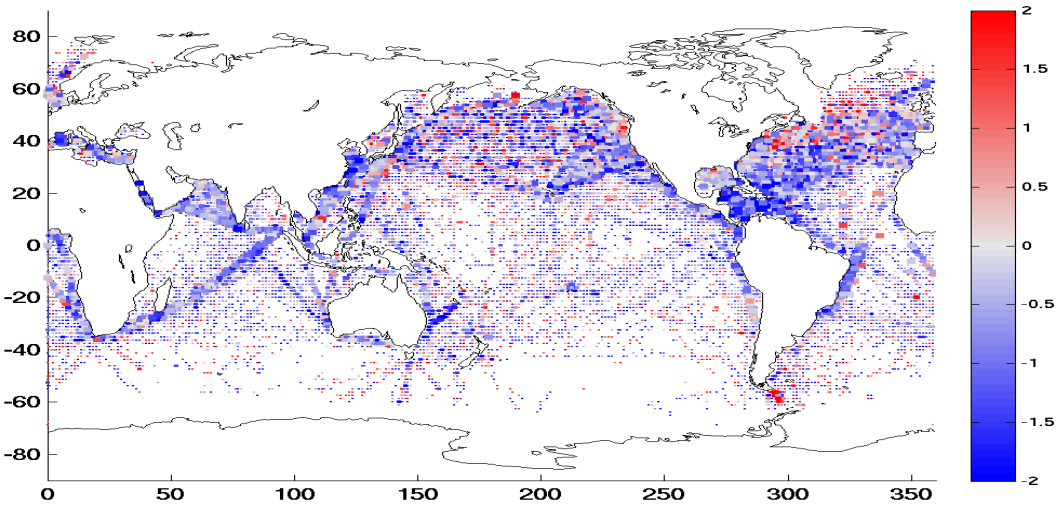

Figure 4- 9: NOGAPS Scalar Wind Speed Bias. The U/V components of the wind were merged to form a scalar speed for comparison purposes to NFLUX. NOGAPS has a negative bias 58% of the time

As indicated in equations (9) and (10) for latent and sensible heat flux, errors in the horizontal wind speed will be directly proportional to the errors in both fluxes. Table 19 shows the confidence limits for the skill score for scalar wind speed.

Table 19: Global NFLUX U10 Skill Score. The performance of the NFLUX U10 product is better than the NOGAPS performance at the 95% CL.

U10	95% Lower CL	Skill Score	95% Upper CL
NFLUX	0.2657	0.2874	0.3124
NOGAPS	0.0548	0.0808	0.1106

4.3.2 WindSat Wind Speed

The low resolution EDRs from WindSat are included in the NFLUX system and are shown in Figure 4- 10. The global skill scores for WindSat and NOGAPS are presented in Table 20.

Table 20: Global WindSat Skill Score. The low resolution WindSat skill score is greater than the NOGAPS scalar wind speed skill score for the match up time periods shown in Figure 3-13.

WindSat	95% Lower CL	Skill Score	95% Upper CL
NFLUX	0.3545	0.3763	0.4031
NOGAPS	0.2573	0.2836	0.2874

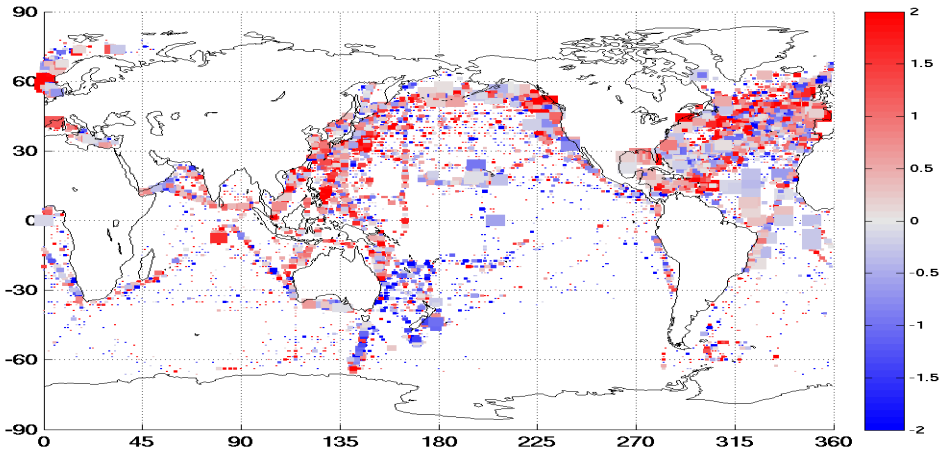

Figure 4- 10: WindSat Global Bias. The global bias for WindSat is 0.73 m s^{-1}. This is reduced to 0.55 m s^{-1} when only observations within ±60^{o} are considered. In this region, the probability that WindSat will be positively biased is 59%.

5 Regional Models

The global bias shown in Figure 4- 4 (Qa), and Figure 4- 6 (Ta) clearly indicate areas where the NFLUX algorithms do not perform as well as they do globally. Several regions of naval interest were selected to use existing techniques to improve the performance of the NFLUX algorithms. These regions are indicated in Table 21 and Figure 5- 1.

Table 21: NFLUX Regional Boundaries. Four regions were selected to use a regional-specific set of coefficients for Qa and Ta.

Region	Latitude Boundary	Longitude Boundary
Arabian Sea	[0 30]	[20 80]
Okinawa	[0 30]	[100 140]
S. China Sea	[18 35]	[120 150]
California	[20 40]	[220 245]

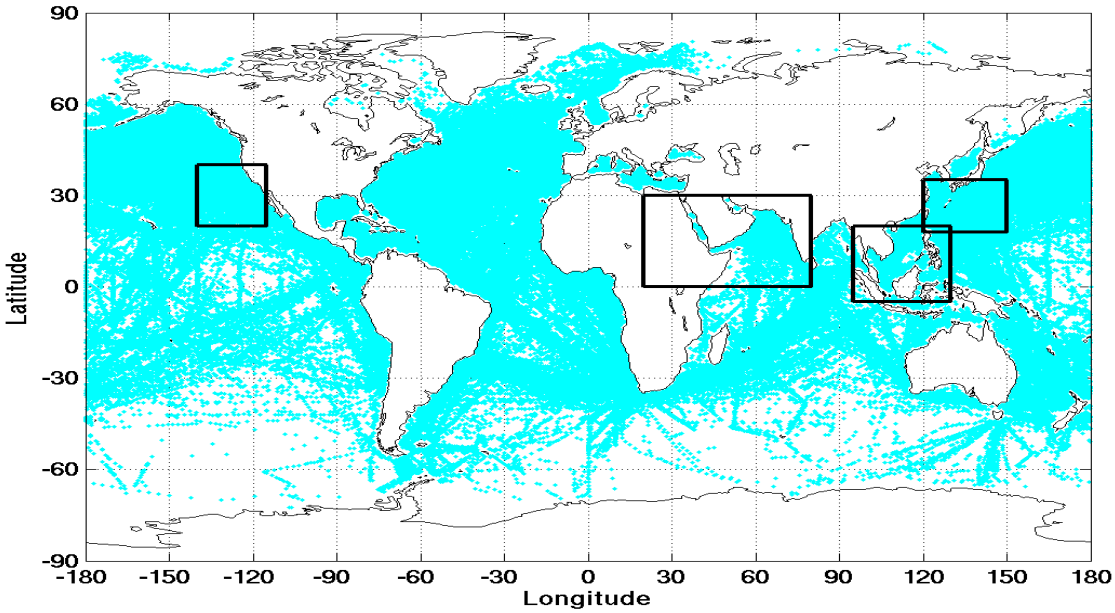

Figure 5- 1: Regional Areas. Four regional areas of naval interest were selected to determine the potential for regional algorithms.

A reduced region results in a much more limited set of match-ups between satellite and *in situ* observations. Initial attempts to merely rerun the algorithm generation program did not yield significant improvements. When the bootstrapping technique was adjusted to allow 10^4 realizations of the algorithm development, convergence of the algorithm coefficients was improved.

The regional algorithm products overlay the existing global product estimate. The location of the observations is tested to see if it falls within one of the regional areas. If the observation is located within a specific region, the global coefficients are swapped out for the regional coefficients and used to calculate either the SST-augmented product or the non-SST product.

Figure 5- 2 through Figure 5- 5 shows the comparison of the Qa bias for the four regions shown in Figure 5- 1. Table 22 shows the comparison of the Qa mean error and skill score pair using the global algorithm, the new regional algorithm, and for comparison purposes, NOGAPS. The improvement in the Arabian Sea, Figure 5- 2, is in the center of the region and along its eastern boundary. The regional algorithm resulted in an improvement of the ME by approximately 0.5g kg^{-1} and a substantial improvement of the skill score, from 0.04 to 0.24.

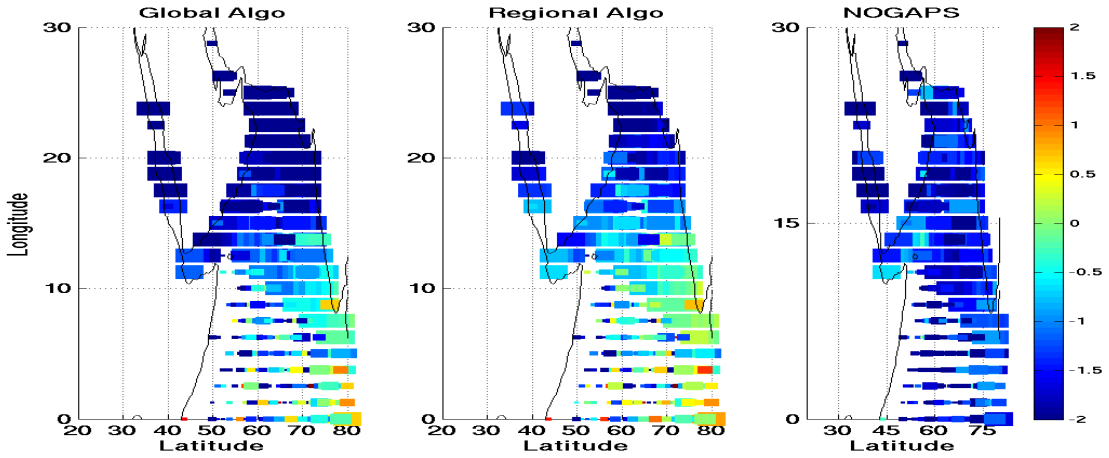

Figure 5- 2: Arabian Sea Qa Regional versus Global Performance. The left panel represents the performance of the global Qa algorithm for SSMIS and AMSU sensors. New algorithms for each satellite were developed for the Arabian Sea and the combined performance of that algorithm is shown in the middle panel. The middle and upper portions of the region show improvement. The skill score was 0.035 and improved to 0.2369.

The Okinawa region, Figure 5- 3, showed some improvement with the use of a regional algorithm. The ME was reduced by over 0.25g kg^{-1}; however, the overall skill score was only improved by a minor amount. The South China Sea, Figure 5- 4, showed a more visible improvement in its bias reduction of 0.1g kg^{-1}. The skill score was improved but remained negative. Equation (7) indicates that when the linear regression is small, in this case 0.33, it is possible to have a negative skill score. The California region, Figure 5-5, did not show any change in either the ME or skill score.

The Arabian Sea is the region that shows the most marked improvement. Most of this improvement comes from the AMSU sensors. The global AMSU Qa algorithm produced an ME of -1.30 g kg^{-1} and a skill score of 0.25. The regional AMSU Qa algorithm produced an ME of -0.17 and a skill score of 0.64. The global SSMIS Qa had an ME of -1.62 and skill score of -0.22. The ME for the regional SSMIS Qa had a higher absolute value at -1.73 with a skill score of -0.08. The R^2 for the global SSMIS Qa was 0.42 and the regional R^2 was 0.47.

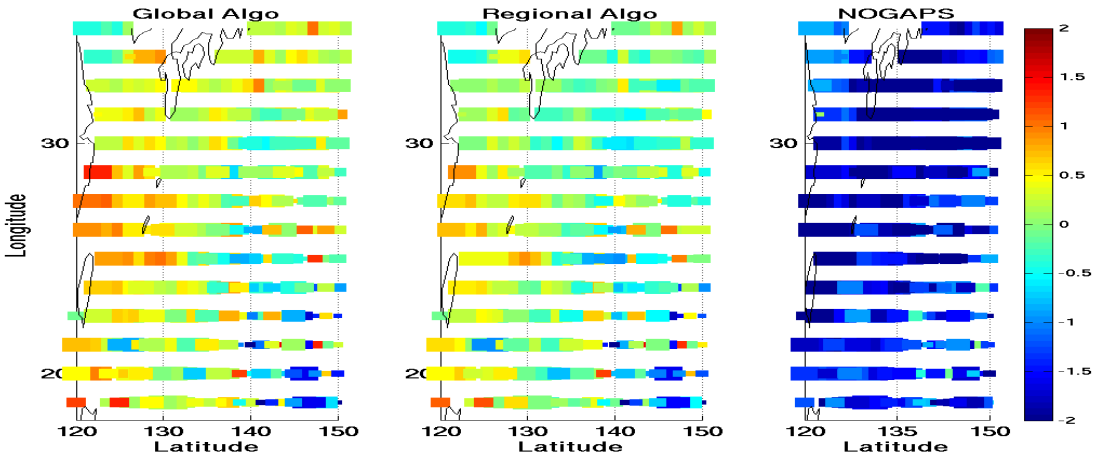

Figure 5- 3: Okinawa Qa Regional versus Global Performance.

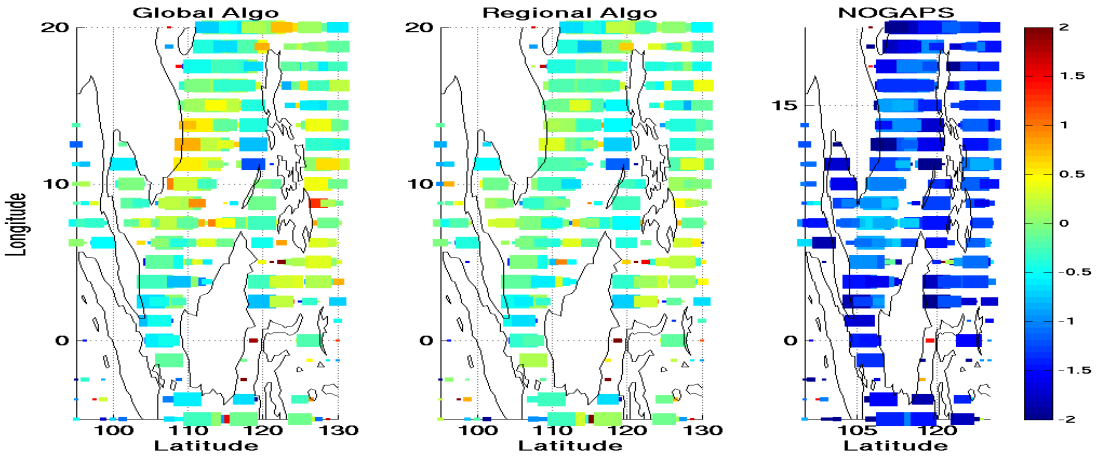

Figure 5- 4: South China Sea Qa Global versus Regional Performance.

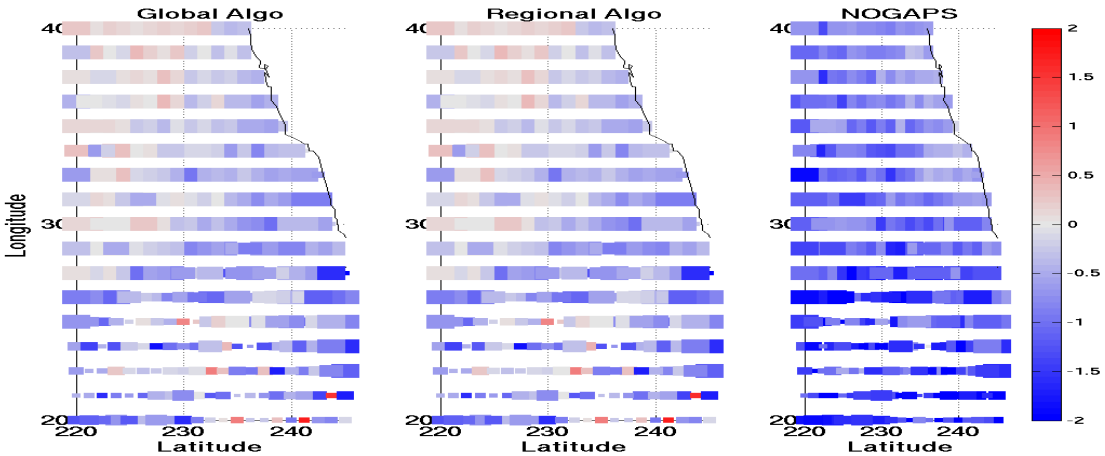

Figure 5- 5: California Qa Global versus Regional Performance.

Table 22: Qa Global and Regional Algorithm Comparisons. The mean error (bias) and the 95% CL for the skill score are shown for the four regions. Only the California region shows no improvement. NOGAPS data is provided for comparison purposes. All values have units of g kg^{-1}.

Region	Global Algorithm ME/Skill Score	Regional Algorithm ME/Skill Score	NOGAPS ME/Skill Score
Arabian Sea	-1.48/0.04	-0.91/0.24	-1.44/0.30
Okinawa	0.34/0.83	0.07/0.84	-1.72/0.72
S. China Sea	0.70/-0.22	0.60/-0.16	-1.22/0.14
California	-0.35/0.37	-0.35/0.37	-0.93/0.22

The regional ME/skill score data pairs for the Ta NFLUX product are shown in Table 23. In every region, except for California, the regional algorithm performed better and in both the Arabian Sea and Okinawa regions, the ME was reduced.

Table 23: Ta Global and Regional Algorithm Comparisons. The mean error (bias) and skill score are shown for the four naval regions of interest. Only California shows no improvement using a regional algorithm. All values have units of ^{o}C.

Region	Global Algorithm ME/Skill Score	Regional Algorithm ME/Skill Score	NOGAPS ME/Skill Score
Arabian Sea	-0.93/0.43	-0.30/0.63	-0.88/0.36
Okinawa	0.43/0.89	-0.10/0.91	-0.69/0.88
S. China Sea	0.13/0.57	-0.14/0.59	-0.28/0.50
California	0.17/0.66	0.17/0.66	0.06/0.75

A small study was conducted on the potential for regional wind speed algorithms. It indicated that an improvement in neither ME nor skill score could be expected in any of the regions. It is unclear if this is the result of insufficient *in situ*/satellite match ups or if there are other processes involved. No regional wind speed algorithms will be utilized.

6 Conclusions

The NFLUX system was developed to provide near-real time observations of the ocean surface for assimilation into operational ocean models. The ocean surface state variables of specific humidity, air temperature, and wind speed are provided by NFLUX PRE at a performance level meeting or exceeding the atmospheric model 1/2^o NOGAPS.

The global performances of the NFLUX products are contrasted with NOGAPS in Table 24. All three of the NFLUX products are critical to the calculation of the heat flux at the ocean surface. The global mean error, or bias, coupled with the global skill score provides an acceptable metric for the entire range of observations. The specific humidity product is the superior product over the 1/2^o NOGAPS forecast model. The wind speed product has a positive ME with a greater magnitude compared to NOGAPS, but its skill score is greater. The air temperature is essentially equal in performance.

Table 24: Global NFLUX Performance. The full range of statistical metrics are provided for the NFLUX product suit and compared to those of NOGAPS. The data is based upon match ups between *in situ* observations and satellite overpasses within 1^o and 6 hours. Units are g kg^{-1} for Qa, ^{o}C for Ta, and m s^{-1} for U10.

Product	NFLUX				NOGAPS			
	ME	SD	RMSE	Skill	ME	SD	RMSE	Skill
Qa	-0.29	1.75	1.77	0.89	-1.07	1.63	1.95	0.86
Ta	-0.24	1.62	1.64	0.98	-0.21	1.62	1.64	0.96
U10	0.62	2.76	2.83	0.29	-0.47	3.18	3.21	0.08

One of the areas of emphasis for NFLUX was the ability to improve the estimates of the products at the higher ranges, shown in Table 25. Table 25 shows that the product performance for air temperature again is essentially equal. However, for both specific humidity and wind speed, the NFLUX product mean error at high values is less than half the NOGAPS forecast mean error.

Table 25: NFLUX High Value Performance. The NFLUX algorithms were developed for the full range of expected data.

Product	NFLUX ME	NOGAPS ME
Qa > 20 g kg^{-1}	-1.20	-2.43
Ta >25^{o}C	-0.50	-0.51
U10 >10 m s^{-1}	-1.06	-2.75

The heat flux will determine the temporal and spatial parameters of the upper ocean, such as the mixed layer depth. Persistent mean errors in the conditions at the ocean surface will result in divergences between the actual conditions and those forecast by the model. The typically smaller, or equal, mean errors of NFLUX compared to NOGAPS are expected to result in improved ocean model performance.

7 References

Fairall, C. W. and Bradley, E. F. and Hare, J. E. and Grachev, A. A. and Edson, J. B. (2003) Bulk parameterization of air-sea fluxes: Updates and verification for the COARE algorithm, Journal of Climate, Vol 16, No. 4, 571-591.

Gilhousen, D.B. (1998). A Field Evaluation of NDNC Moored Buoy Winds., Journal of Atm. And Oceanic Tech., Vol 4, 94-104.

Goldberg, M. D. and Crosby, D. S. and Zhou, L. H. (2001). The limb adjustment of AMSU-A observations: Methodology and validation, Journal of Applied Met.,, Vol 40, No. 1, 70-83

Goodberlet, M. A., C.T. Swift, J.C. Wilkerson (1989). Remote sensing of ocean surface winds with the special sensor microwave/imager, JGR, Vol 94, No. C10, 14547-14555.

Goodberlet, M.A., Swift, C. T. (1992). Improved Retrievals from the DMSP Wind-Speed Algorithm under Adverse Weather Conditions, IEEE Trans. on Geosci and Remote Sensing, Vol 30, No. 5, 1076-1077.

Goodberlet, M.A., Swift, C. T., and Wilkerson, J.C. (1990). Ocean Surface Wind-Spped Measurements of the Special Sensor Microwave Imager (SSM/I). IEEE Trans. on Geosci and Remote Sensing, Vol 28, No. 5, 823-828

Grody, N.C. (1991). Classification of Snow Cover and precipitation Using the Special Sensor Microwave Imager, JGR, Vol 96, No. D4, 7423-7435.

Grody, N.C., F. Weng, and R.R. Ferraro, (1999). Application of AMSU for Obtaining Hydrological Parameters, Microwave Radiometry and Remote Sensing of the Earth's Surface and Atmosphere. VNU Science Press, Brill Academic Publishers, Inc., 339-351.

Hu, J-C., W-J. Chen, C-C. Li, C-C. Chao, (2006). Rainfall Estimation of Mesoscale convetive Ssytems Using AMSU-A Data during the Mei-Yu Season, TAO, Vol 17, No 1, 91-109.

Hwang P.A. (2012). Foam and Roughness Effects on Passive Microwave Remote Sensing of the Ocean, IEEE Trans. on Geoscience and Remote Sensing, Vol 50, NO. 8 2978-2985.

Jackson, D.L., G.A. Wick, and J.J. Bates (2006). Near-surface retrieval of air temperature and specific humidity using multisensor microwave satellite observations, JGR, Vol 111, D10, pp 16.

Jackson, D. L., G. A. Wick, and F. R. Robertson (2009). Improved multisensor approach to satellite-retrieved near-surface specific humidity observations, J. Geophys. Res., 114, D16303, doi:10.1029/2008JD011341.

Karbou, F., P. Bauer, A. Geer, and W. Bell, Exploitation of microwave sounder/imager data over land surfaces in the presence of clouds and precipitation, http://hsaf.meteoam.it/documents/reference/VS-37-ECMWF-Karbou-final-report.pdf, accessed 26OCT2012.

Kent, E. C. and Berry, D. I. (2005). Quantifying random measurement errors in Voluntary Observing Ships' meteorological observations, Int. J. Climatol., 25: 843–856.

Kent, E.C., S.D. Woodruff, D.I. Berry, (2007). Metadata from WMO Publication No. 47 and an Assessment of voluntary Observing ship Observation Heights in ICOADS", Journal of Atm. and oceanic Tech, Vol 24, 214-234

Mo, T. (1999). AMSU-A Antenna Pattern Corrections, IEEE Trans. on Geosci. and Remote Sensing, Vol. 37, No. 1, 103-112.

Murphy, A.H. (1988). Skill Scores on the Mean Square Error and Their Relationships to the Correlation Coefficient, Monthly Weather Rev., Vol 116, 2417-2424.

Murphy, A.H. (1995). The Coefficients of Correlation and Determination as Measures of Performance in Forecast Verification, Weather and Forecasting, Vol 10, 681-688.

8 Acronyms and Abbreviations

Acronym	Description
AMSU	Advanced Microwave Sounding Unit
ATMS	Advanced Technology Microwave Sounder
COARE	Coupled Ocean-Atmosphere Response Experiment
DMSP	Defense Meteorological Satellite Program
EDR	Environmental Data Records
FOV	Field of View
GTS	Global Telecommunications System
MHS	Microwave Humidity Sounder
MLR	Multi-linear Regression
NCODA	Navy Coupled Ocean Data Assimilation
NDBC	National Data Buoy Center
NESDIS	NOAA National Environmental Satellite, Data and Information Service
NFLUX	NRL Ocean Surface Flux
NPOESS	National Polar-orbiting Operational Environmental Satellite System
NPP	National Polar-orbiting Partnership, ex- NPOESS Preparatory Project
POES	Polar Orbiting Environmental Satellites
Qa	Specific Humidity
QC	Quality-Controlled
RMSE	Root Mean Square Error
RTDHS	Real Time Data Handling System
SDR	Sensor Data Records
SI	Scattering Index
SSMIS	Special Sensor Microwave Imager/Sounder
SST	Sea Surface Temperature
STAR	Center for Satellite Applications and Research
Ta	Surface Air Temperature
Tb	Brightness Temperature
U	Surface Wind Speed
WMO	World Meteorological Organization